NASA CR-143843

EFFECTS OF CONTROL LAWS AND RELAXED STATIC STABILITY ON VERTICAL RIDE QUALITY OF FLEXIBLE AIRCRAFT

Philip A. Roberts, Robert L. Swaim,
David K. Schmidt, and Andrew J. Hinsdale

Purdue University
West Lafayette, Indiana 47907

April 1977

Prepared for

NATIONAL AERONAUTICS AND SPACE ADMINISTRATION
Dryden Flight Research Center
Edwards, California 93523

1. Report No.	2. Government Accession No.	3. Recipient's Catalog No.
NASA CR-143843		

4. Title and Subtitle	5. Report Date
EFFECTS OF CONTROL LAWS AND RELAXED STATIC STABILITY ON VERTICAL RIDE QUALITY OF FLEXIBLE AIRCRAFT	April 1977
	6. Performing Organization Code

7. Author(s)	8. Performing Organization Report No.
Philip A. Roberts, Robert L. Swaim, David K. Schmidt, and Andrew J. Hinsdale	H-962
	10. Work Unit No. 505-06-91
9. Performing Organization Name and Address	11. Contract or Grant No.
Purdue University West Lafayette, Indiana 47907	NSG 4003
	13. Type of Report and Period Covered
12. Sponsoring Agency Name and Address	Contractor Report - Topical
National Aeronautics and Space Administration Washington, D.C. 20546	14. Sponsoring Agency Code

15. Supplementary Notes

NASA Technical Monitor: Donald T. Berry, NASA Dryden Flight Research Center

This report is substantially the same as the first author's doctoral dissertation, which was published under the same title by the School of Aeronautics and Astronautics at Purdue University.

16. Abstract

Control configured vehicle technology has evoked a quantum advance in the capability to control various performance aspects of aerospace vehicles. In the past, ride quality, as a performance area, has received minimal attention in the design phase. With this new capability available, definitive ride quality specifications and rules are needed for the initial design phases. State variable techniques are utilized herein to generate the RMS vertical load factors for the B-52H and B-1 bombers at low level, mission critical, cruise conditions. A ride quality index is proposed to provide meaningful comparisons between different controls or conditions. Ride quality is shown to be relatively invariant under various popular control laws. Handling quality variations are shown to be major contributors to ride quality variations on both vehicles. Relaxed static stability is artificially implemented on the study vehicles to investigate its effects on ride quality. The B-52H ride quality is generally degraded when handling characteristics are automatically restored by a feedback control to the original values from relaxed stability conditions. The B-1 airplane shows little ride quality sensitivity to the same analysis due to the small rigid body contribution to load factors at the flight condition investigated.

17. Key Words (Suggested by Author(s))	18. Distribution Statement
Ride quality Flexible aircraft Control laws Handling qualities Relaxed static stability	Unclassified - Unlimited Category: 08

19. Security Classif. (of this report)	20. Security Classif. (of this page)	21. No. of Pages	22. Price*
Unclassified	Unclassified	109	

For sale by the National Technical Information Service, Springfield, Virginia 22161

TABLE OF CONTENTS

LIST OF TABLES

LIST OF FIGURES

LIST OF SYMBOLS

Abbreviations

CCV	Control configured vehicle
CPU	Central processing unit
NASA	National Aeronautics and Space Administration
RMS	Root mean square
RQ	Ride quality
RQI	Ride quality index
RSS	Relaxed static stability
SMCS	Structural mode control system
USAF	United States Air Force

Referentials

A	Matrix of physical state coefficients in the vehicle equations of motion
a_{ij}	Matrix element located in the ith row and jth column
a_z	Acceleration in the positive z direction
B	Matrix of control variable coefficients in the vehicle equations of motion
b	Wing span
C*	Blended pitch rate and vertical acceleration control law, also called: "C star"
cg	Center of gravity
D	Derivative operator

d_i	Open loop characteristic equation coefficients
$E\{\cdot\}$	Expected value
E_i	Total area under the load factor curve for the ith control case
e_i	Closed loop characteristic equation coefficients
$e^{M\tau}$	State transition matrix
F	Sum of all applied forces; Generalized force
ft	Feet
G	Scalar white noise coefficient vector in the vehicle equations of motion
g	Local gravitational acceleration (9.80 m/sec^2 (32.17 ft/sec^2))
H	Angular momentum vector
In	Inches
K	Gain (scalar or matrix) value(s) which multiplies the control feedback variables
k	Gain matrix representing the matched coefficient differences between the closed and open loop characteristic equations
L	Gust scale length
ℓ	Distance from center of gravity along the fuselage centerline, positive forward, m (ft)
M	Sum of all applied moments
M_q	Change in moment due to pitch rate $(\frac{1}{sec})$
M_{δ_e}	Change in moment due to elevator deflection $(\frac{1}{rad\text{-}sec^2})$
M_w	Change in moment due to vertical velocity, $\frac{1}{m\text{-}sec}$ $(\frac{1}{ft\text{-}sec})$
$M_{\dot{w}}$	Change in moment due to acceleration along the z axis $\frac{1}{m}$ $(\frac{1}{ft})$
$\bar{m}$	Number of elastic modes included in the load factor expression

m	Meters
N	Vertical load factor normalized with local gravity (g's/ft/sec or g's/.3m/sec)
n	Number of states in the vector x
p	Linear momentum vector
$P(\ell)$	Deterministic row vector which is a function of fuselage station; generates the instantaneous load factor when multiplied times the state vector
q_g	Perturbation pitch angle rate of change (same as $\dot{\theta}$) due to variations in vertical gust properties along the centerline of the vehicle (rad/sec)
rad	Radian(s)
sec	Second(s)
T	Similarity transform matrix which produces the phase variable canonical form matrix
t	Time (sec)
t_i	Similarity transform matrix, ith column vector
U	Steady state vehicle velocity
u	Matrix of control elements
w	Perturbation vertical velocity, positive down along z axis
x	Column vector of states associated with the physical output states of the aircraft
x_g	Column vector of gust state variables
$\|Z\|$	Determinant of a matrix, Z
Z_w	Change in vertical force due to vertical velocity $(\frac{1}{sec})$
Z_{δ_e}	Change in vertical force due to elevator deflection, $\frac{m}{rad\text{-}sec^2}$ $(\frac{ft}{rad\text{-}sec^2})$

Greek

α	Perturbation angle of attack (rad)
α_g	Perturbation angle of attack change due to a vertical gust (rad)
α_{g_1}	Non-physical dummy state for the time domain turbulence representation
γ	Perturbation flight path angle (rad)
δ_e	Elevator deflection (rad)
ζ	Damping
η	Scalar unit white noise, time domain representation
θ	Perturbation pitch angle (rad)
ξ_i	Generalized coordinate of the ith elastic mode
$\sum$	Summation operator
Φ	Power spectra function
$\phi_i(\ell)$	Orthogonal elastic mode shape, ith elastic mode value at fuselage position ℓ.
ω	Frequency (rad/sec)

Subscripts

avg	Average (mean) value
BL	Base line value, used with the ride quality metric
g	Gust related value or variable
max	Maximum value
min	Minimum value
n	Natural frequency
R_5, R_6,...	Row 5, Row 6 and so on of a particular matrix
rms	Root mean square value or variable
SP	Short period

Superscripts

Q'	Transpose of a matrix; the matrix Q is used here only as an example
$\overline{Q}$	Modified matrix
$\dot{Q}$	Derivative with respect to time of Q
Q^{-1}	Matrix inverse
Q^*	Augmented matrix; implies the addition of more states or control variables

Chapter 1

INTRODUCTION

1.1 Control Configured Vehicles

The advent of Control Configured Vehicle (CCV) technology has changed the design process for modern aerospace vehicles and promises important improvements in future advanced control capabilities. CCV technology includes important performance areas such as flutter mode control, relaxed static stability, ride control, fatigue reduction, gust load alleviation, and maneuver load control. This research endeavor will focus on Ride Quality (RQ) and its design sensitivity to various types or states of control philosophies. For this study RQ is defined as the RMS (root mean square) normal acceleration level which the vehicle manifests when subjected to cruise condition unit turbulence intensities.

1.2 Ride Quality History and Import

Systematic review of flight vehicle design history reveals that payload, range, cost, speed, maneuverability, handling characteristics, and economic factors were the primary guidelines which structured a final production vehicle. Until the mid-1960's the vehicle RQ was determined by structural fatigue constraints, the right kind of passenger seat padding, and whatever pilot handling characteristics were required for the vehicle. In retrospect RQ was handled after the vehicle was produced by reducing passenger awareness of vibrations or discomforts. This was accomplished through various mental or physical activities (including alcoholic beverages) designed as diversions. Design history is about to undergo another quantum jump in capability.

The availability of mini-computers, fly-by-wire, and active control technologies are necessary for this new capability in design. The

melding of optimal solution techniques with traditional design groups like structures, aerodynamics, controls, and propulsion is providing iterative design capabilities which promise great economy, efficiency, and marketability for future aerospace vehicles. More specifically it will not only be feasible to design vehicles to certain RQ specifications, but the physics and economics of design will force RQ to be a design constraint.

From the economic point of view, future aerospace designs must provide a range of RQ to the commercial vehicle consumers. The consumer companies or government contractors will then have a management decision capability in determining what the market (or mission) will support or need. The times when the consumers were forced to accept whatever RQ they could get are now past.

The physics of design will force RQ into the picture. Each new design vehicle seems to show one important trend. As total gross take-off weight spirals upward, empty weight remains at least the same as the last generation vehicles or in some cases is dramatically lowered. This phenomena is due to composite materials, better structural design, and high lift technology. It ultimately results in considerably more elastic effects on RQ. This effect is epitomized by the B-1 bomber used in this study.

These elastic contributions are exhibiting a tendency toward lower undamped natural frequencies. Thus large flexible vehicles of the future will probably be subject to rigid body/elastic mode interactions. This problem must be investigated before such difficulties are physically encountered. When the short period frequency and lower frequency elastic modes begin to interface, these interactions will certainly affect the pilot's assessment of the handling qualities. Therefore, some logical study of these elastic effects and revised design standards must be inaugurated for large flexible vehicles. To date no design criteria exist for RQ in terms of control system specifications. It is hoped that this thesis will be a basic step in that direction.

1.3 RQ Design Parameters

The deficiency and usual omission of RQ design constraints demonstrates the critical need for research in this area. Some of the most recent work includes the Boeing B-52E/F CCV studies performed under contract with the USAF Flight Dynamics Laboratory, reference 13. These studies and test flights demonstrated the feasibility of ride smoothing (control of RQ) and showed that it was compatible with other CCV performance areas.

In another research effort I.D. Jacobsen and others at the University of Virginia are gathering evidence for integrated RQ expressions utilizing three dimensional acceleration information. Through statistical comparisons of actual turbulent conditions with passenger reactions, their correlation studies are showing trends toward certain theoretical ride comfort expressions (reference 11).

More recently Rockwell International introduced the B-1 which has a Structural Mode Control System (SMCS) consisting of two symmetrically opposite vanes on the forward fuselage. The SMCS serves basically as a ride control system. This system is required because of the highly elastic properties exhibited by the basic vehicle. The question arises then, could an active control with appropriate programming utilize normal control surfaces and achieve the same effects? If so, what control philosophy would be best? And last, but maybe most important, what are the cost benefits of this capability?

To provide a systematic approach toward RQ design, Dr. Robert Swaim proposed and received funding from NASA Dryden Research Center, Edwards AFB, CA., for the study of:

1. RQ Sensitivity to Type of Control Philosophy
2. RQ Effects Under Relaxed Static Stability Implementations
3. Effects of Dynamic Elasticity on Handling Qualities and Pilot Rating
4. Sensitivity of SAS Designs to Uncertainties in the Mathematical Models of Elastic Modes.

The first two parts of Dr. Swaim's proposal were used as research topics for this thesis.

1.4 Relaxed Static Stability

Control philosophies such as rate feedback are familiar topics with the modern engineer. Relaxed static stability is rather new when used as a "variable" in the preliminary design process. Therefore it deserves a brief introduction.

Relaxed Static Stability (RSS) is herein defined as the reduction or elimination of inherent aerodynamic static and dynamic vehicle stability requirements. An active control system is used to restore or maintain desired stability and handling characteristics. This CCV performance area is destined to be the first flight-critical concept used in the next generation of advanced cargo or large commercial vehicles. Since the supersonic transport studies were completed, various payoff and trade studies on RSS have shown great promise in specific fuel consumption parameters. The RSS concept is currently incorporated in the design of the new F-16 fighter that the USAF selected as its next generation lightweight combat airplane. The trends in fossil fuel availability and price indicate that RSS will necessarily be an integral part of advanced vehicle design.

1.5 Objectives

The overall objective of this work is a clear statement of the effects on vertical RQ when control philosophy or RSS changes are incorporated on the study vehicles. It is hoped that this study will lead to specific RQ design standards that are realizable and practical for future aerospace vehicles. It was necessary that some comparative parameter be found that would quantify good and bad RQ. Hence, a secondary but fundamental objective was finding a metric that would judge RQ according to some predetermined philosophy.

1.6 Organization

This thesis is divided into four investigative chapters. The next chapter is designed as a review of ride quality and suggests the metric which will discriminate between various vertical acceleration curves representing ride quality. Chapter 3 is devoted to a parametric study

of control law effects on RQ. Chapter 4 delves into handling quality specifications and their effects. Chapter 5 reviews the static stability effect and traces its impact on the vertical load factors of the B-1 and B-52H. The summary, results, and conclusions as well as further research recommendations are included in Chapter 6. The three appendices provide basic vehicle flight condition data, a complete listing of the study cases, and a section on interesting computational aspects.

Chapter 2

VERTICAL RIDE QUALITY

2.1 Definition and Model.

Since general RQ in terms of passenger comfort has successfully eluded analytical representation to this date, RQ will be defined in this thesis as the RMS load factor curve along the fuselage centerline of the study vehicles. Equation 2.1 represents the vertical load factor at station ℓ of the centerline.

$$N(\ell,t) = \frac{1}{g}\left[U\,\dot{\gamma}(t) + \ell\,\ddot{\theta}(t) - \sum_{i=1}^{\bar{m}} \phi_i(\ell)\,\ddot{\xi}_i(t)\right] \qquad (2.1)$$

where:

N		the local gravity normalized load factor
ℓ		the distance from the cg, positive forward
t		time
U		steady state forward velocity
γ		the perturbation flight path angle
θ		the perturbation pitch angle
$\phi_i(\ell)$		the ith orthogonal elastic mode shape value at station ℓ
$\bar{m}$		the number of elastic modes included
ξ_i		the generalized coordinate of the ith mode
g		the local gravitational acceleration

This simplified load factor expression assumes trimmed cruise conditions with no lateral coupling.

Throughout this paper reference will be made to "rigid body only" load factor contributions to RQ. Unless otherwise noted this situation implies the omission of the summation term in equation 2.1. It should be pointed out that the rigid body physical output variables remaining

are still coupled to the elastic degrees of freedom in the vehicle equations of motion. Hence, the vehicle response dynamics are still elastic.

The study vehicle equations of motion are arranged with physical variables as the states shown in Appendix A. Recalling equations A.8 and A.9:

$$\dot{x} = Ax + Bu + G\eta \tag{A.8}$$

$$x' = \left| \xi_1 \; \xi_2 \; \xi_3 \; \xi_4 \; \alpha \; \dot{\theta} \; \dot{\xi}_1 \; \dot{\xi}_2 \; \dot{\xi}_3 \; \dot{\xi}_4 \; \alpha_{g_1} \; \alpha_g \; q_g \right| \tag{A.9}$$

where:

ξ_i	the ith mode generalized coordinate
α	the perturbation angle of attack
θ	the perturbation pitch angle
α_{g_1}	the dummy gust state
α_g	the change in angle of attack due to a vertical gust
q_g	the change in pitch rate due to a vertical gust, penetration effect
x	the state vector (13 x 1)
u	the elevator control (δ_e)
η	scalar unit white noise
A	state coefficient matrix (13 x 13)
B	control coefficient matrix (13 x 1)
G	gust forcing coefficient matrix (13 x 1)

The sign convention used throughout this work is the standard right-handed stability axis system with origin at the vehicle center of gravity and the x axis positive forward along the centerline. A drawing of the stability axis system is shown in Figure 2.1.a. The y axis is positive toward the right wing tip and the z axis is positive down. The load factor will be positive in the positive z direction. The sign convention for the generalized coordinates and mode shapes of symmetric fuselage modes is shown in figure 2.1.b.

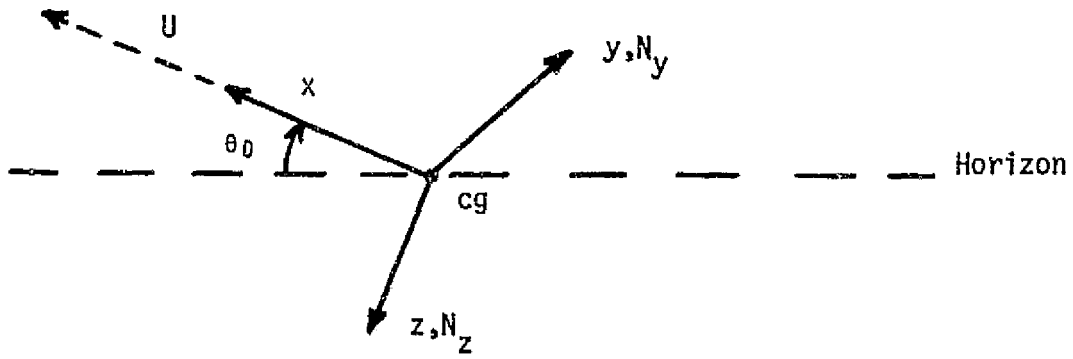

a: Stability Axis System

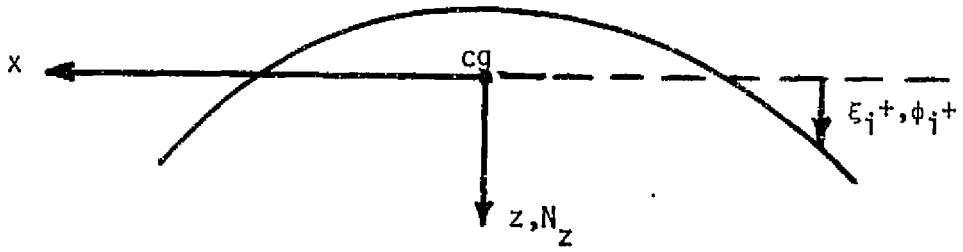

b: Fuselage Vertical Bending

Figure 2.1 Sign Conventions.

2.2 RMS Load Factors and Solution Technique

To determine RQ the RMS load factor is used throughout this work. We are seeking a response to unit turbulent excitation for mission- or vehicle-critical flight conditions. For this thesis the B-52H and B-1 flight conditions satisfy the critical condition requirement. To generate the RMS load factor several matrix and operator manipulations are required. The load factor equation 2.1 can be reconstituted in a state variable format 2.2:

$$N(\ell,t) = P(\ell)\, x(t) \tag{2.2}$$

The row vector $P(\ell)$ is (1xn) where n is the number of states in the gust augmented x vector. From the state vector equation A.8 we can expand slightly to see that:

$$\dot{x} = Ax + Bu + G\eta \tag{A.8}$$

The fifth equation:

$$\dot{\alpha} = A_{R_5}x + B_{R_5}u + 0\cdot\eta \tag{2.3}$$

The sixth equation:

$$\ddot{\theta} = A_{R_6}x + B_{R_6}u + 0\cdot\eta \tag{2.4}$$

The jth generalized coordinate equation:

$$\ddot{\xi}_j = A_{R(6+j)}x + B_{R(6+j)}u + 0\cdot\eta \tag{2.5}$$

The pitch rate state is the 6th column of A:

$$\dot{\theta} = \lfloor 0\ 0\ 0\ 0\ 0\ 1\ 0\ 0\ 0\ 0\ 0\ 0\ 0 \rfloor x \tag{2.6}$$

For a given control ($u = -Kx$) and a specified gain K on that control, the row vector P is deterministic. Only the states are now subject to statistical uncertainty in that they are forced by random turbulence modeled as shown in Appendix A, equation A.6.

The turbulence model used for this study is the Dryden model in a state vector format. The state vector model is due to Heath and is fully discussed in reference 8. Power spectral density representations of the vertical and pitch gust statistics for clear air turbulence are utilized in transfer function format to generate first order differential equations representing the appropriate aerodynamic force changes. Appendix A gives the power spectral density forms and the resulting differential equation set.

Squaring equation 2.2, rearranging the terms, and using the linear expected value operator produces equations 2.7 which represent the mean square and RMS load factor:

$$E\{N^2\} = PE\{xx'\}P' \tag{2.7a}$$

$$N_{rms} = \sqrt{E\{N^2\}} \tag{2.7b}$$

If we can calculate the covariance matrix of the states, then the RMS load factor value is the square root of 2.7a.

Returning to the state equation A.8, we assume that the gain and control is now specified. Then A.8 becomes 2.8:

$$\dot{x} = A^*x + G\eta \tag{2.8}$$

where A* denotes the matrix augmented with the specified control values

Constructing the transpose of 2.8 and pre-multiplying by x yields 2.9a. Post-multiplying by x' gives 2.9b:

$$x\dot{x}' = xx'A^{*\prime} + x\eta G' \tag{2.9a}$$

$$\dot{x}x' = A^*xx' + G\eta x' \tag{2.9b}$$

Adding:

$$D\{xx'\} = A^*xx' + xx'A^{*\prime} + x\eta G' + G\eta x' \tag{2.10}$$

Under the assumptions that this process is statistically stationary with a zero mean, the derivative of E{xx'} is identically zero. Equation 2.10 can be rewritten:

$$0 = A^*E\{xx'\} + E\{xx'\}A^{*'} + E\{xn\}G' + GE\{nx'\} \qquad (2.11)$$

Bryson and Ho have shown in reference 1 that $E\{xn\} = \frac{G}{2}$ and that $E\{nx'\} = \frac{G'}{2}$ for a unit Gaussian white noise process. Thus equation 2.11 reduces to a linear covariance equation of the form 2.12:

$$A^*E\{xx'\} + E\{xx'\}A^{*'} + GG' = 0 \qquad (2.12)$$

The solution for a 16x16 system can be obtained on the Purdue University CDC 6500 in approximately 30 seconds. The algorithm has been tested and used up to 16 x 16 matrix sizes. The numerical technique used for this solution is suggested by Gelb and others in reference 2. The technique in actual use is an unpublished modification suggested by Dr. David Schmidt, Purdue University, School of Aeronautics and Astronautics.

The stopping condition used in this algorithm deserves some explanation. Since the main diagonal terms are dominant in the equation, the maximum diagonal element on the right hand side in every trial solution was discerned and saved. At the next trial solution this value was compared to the last trial value for convergence tendencies and was assigned a percentage convergence value based on the corresponding element value in the covariance matrix. When the trial solution maximum error was less than 5%, the solution was considered complete. An outline of this method appears in Appendix C.

Now that the covariance matrix E{xx'} is known, the load factor problem is completed by matrix multiplications as shown in equation 2.7.

As each individual sequence of this solution technique was proven, test cases were run on the CDC 6500 to verify computational feasibility and utility. The load factor curves were compared with references 13 and 14 to insure the results were reasonable.

2.3 The Study Vehicles

The B-52H and B-1 were chosen for this study because they exemplify the trend toward more elastic structures for future large vehicles. The B-52, and commercial derivatives thereof, was a member of the first generation of elastic vehicles. Since that era, improved structural design techniques and composite materials have made possible advanced vehicles like the highly elastic B-1.

The flight conditions were chosen because they represent cruise conditions which are mission essential, and because turbulence encounters at low altitudes must be included in design considerations.

The B-52H is used by the U.S. Air Force as a long range bomber. It is 47.55 meters (156 ft) long and has a wing span of 56.4 meters (185 ft). Originally designed as a high altitude bomber, it must now cope with penetration problems by combined high/low altitude profiles. Table 2.1 describes the flight condition for the B-52H.

TABLE 2.1: B-52H Flight Condition

Mass = 158,757 kilograms (350,000 lbs.)
Mach = .55
Velocity = 185.56 meters/sec (608.8 fps)
cg at fuselage station 21.74 meters (855 inches)
Altitude = 609.6 meters (2000 ft)

The B-1 is currently being test flown in a major pre-production effort by Rockwell International and the USAF. It is designed as the replacement vehicle for the aging B-52 fleet. The advanced structures and integrated technology make this vehicle an outstanding example for load factor contributions due to elasticity. The overall length of the B-1 is 46 meters (151 ft). The reference wing span utilized at the flight condition in Table 2.2 is 41.8 meters (136.7 ft).

TABLE 2.2: B-1 Flight Condition

Mass = 103,315 kilograms (227,770 lbs)
Mach = .85
Velocity = 289.4 meters/sec (949.45 fps)
cg at fuselage station 40.67 meters (1061.2 inches)
Altitude = 30.48 meters (100 feet)

2.4 A Ride Quality Index

Some metric is now required to compare the resulting load factor curves. The latest work in this area by Rustenburg (reference 9) relates pilot tracking error to vibration levels. The result is a suggested specification for pilot experienced vibrations. Jacobsen (reference 11) is investigating mathematical relationships between subjective comfort statements and environmental variables on commercial passenger flights. However, no standardized specification exists for RQ in today's design guides such as MIL-F-8785B, "Military Specification - Flying Qualities of Piloted Airplanes", reference 16. As a minimum, this thesis is predicated on the ability to compute and compare the vertical RQ for the B-52H and B-1. It is also hoped that a more general usage for the suggested RQI (Ride Quality Index) can be justified.

As a first level requirement, the RQI must be discriminating for the vertical and lateral decoupled cases. Application to the coupled cases would then logically follow the weighting suggested by Jacobsen. With this requirement, an examination of a typical vertical load factor curve (Figure 2.2) for the B-52H reveals these preliminary observations about the ride in terms of RMS load factors.

Observation 1: The area under the load factor curve is a representation of the energy dissipated by the vehicle when disturbed by unit intensity turbulence.

Observation 2: The maximum and minimum load factors indicate the dispersion along the structure of better or worse acceleration conditions.

Observation 3: The mean load factor value indicates some average level of acceleration experience.

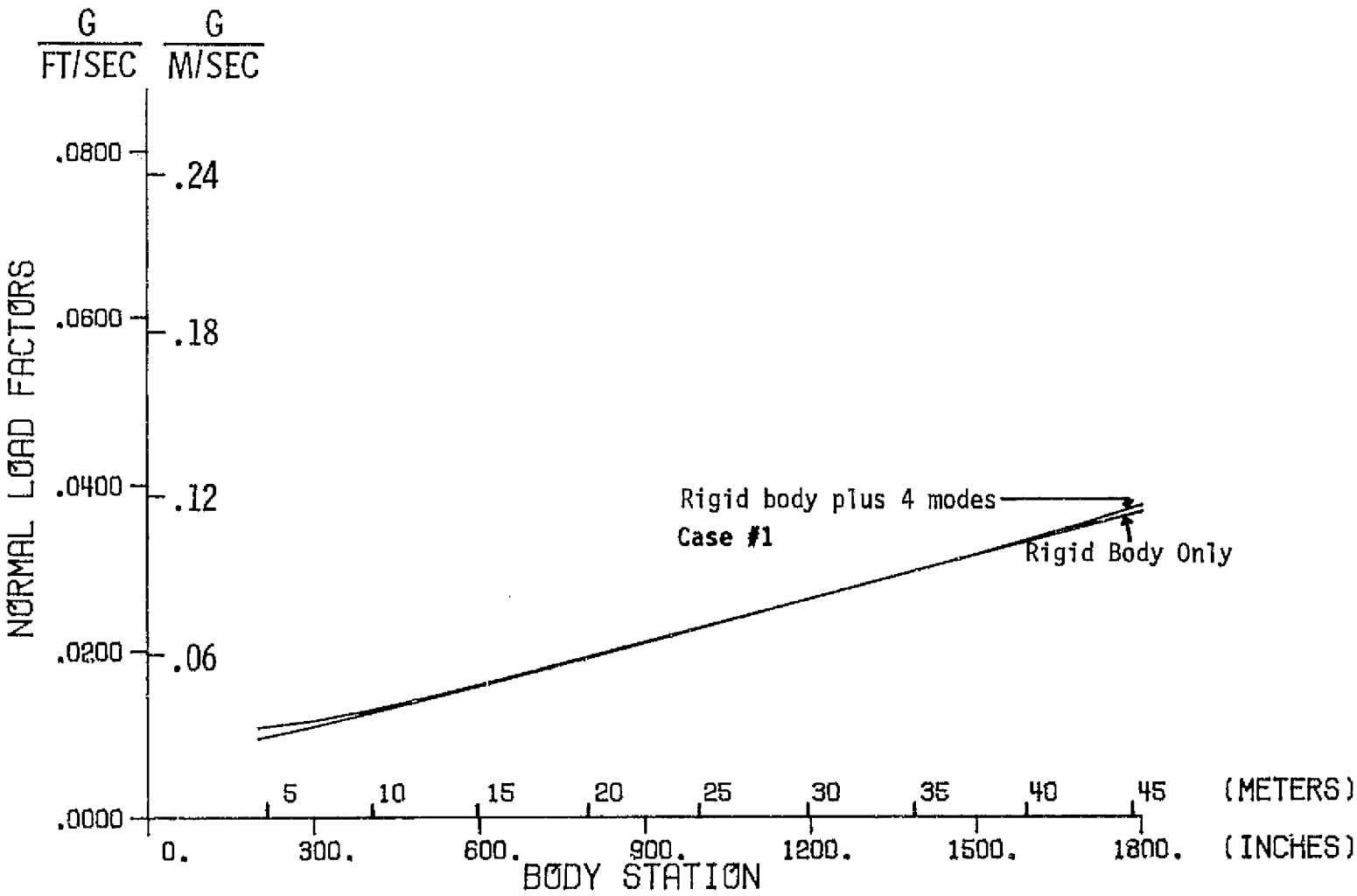

Figure 2.2 B-52H Unaugmented Vehicle Load Factor Curve.
Mach .55, Altitude 610 m (2000 ft).

In addition to these observations some reasonable assumptions can be invoked to decrease RQI complexity.

Assumption 1: The structure is at least quasi-continuous along the fuselage centerline.

Assumption 2: Control law complexity is directly proportional to control implementation cost and exhibits discrete cost jumps relative to the type of control policy used.

Assumption 3: The probability for acceptance of an RQI is inversely proportional to its complexity.

Assuming that a merit value can be assigned to various rides, the most important assumption mentioned above is that simplicity encourages acceptance and use. Following this reasoning I propose the ride quality metric as equation 2.13:

$$RQI = \left[\frac{E_i}{E_{BL}} + \frac{N_{max_i}}{N_{max_{BL}}} + \frac{N_{min_i}}{N_{min_{BL}}} + \frac{N_{avg_i}}{N_{avg_{BL}}}\right]\left[\frac{1}{4}\right] \qquad (2.13)$$

The terms in 2.13 are defined as follows:

E_i total area under the load factor curve for the ith control case

N_{max_i} maximum load factor value for the ith control case

N_{min_i} minimum load factor value for the ith control case

$N_{avg_i} = \frac{\Sigma N_j}{j}$ mean load factor value for the ith control case

The subscript BL represents the baseline value used for the comparison, N_j the load factor value at the j^{th} fuselage lumped mass point, and j^J the number of fuselage mass points.

The baseline values take on special meaning for preliminary design purposes. For example, after the production decision model is well developed, the baseline values could be changed to indicate a marketing value of RQ to the consumer. A brief scenario of the marketing aspect will be included at the end of this chapter.

2.5 Testing and Justification of the RQI

The success of this metric for preliminary design use must certainly be tied to its ability to discriminate and inform design decision managers about the RQ of a current design iteration. The metric is not intended to be an absolute scaling function. However it must inform the manager about RQ in relation to all the other design tradeoffs.

As an example Figure 2.3 shows the load factor curve for the unaugmented (no stability augmentation system) B-1. This model does not include the structural mode control system which the B-1 utilizes in its present configuration.

These load factor curves were generated as described in equation 2.7. The variables E_{BL}, $N_{max_{BL}}$, $N_{min_{BL}}$, and $N_{avg_{BL}}$ are assigned to equation 2.13 from the curve with all four modes. A quick calculation of the RQI for this initial (i = 0) case reveals the RQI is unity. With unity as the comparative point it follows that the RQI equal to zero would represent a "perfect" ride and an RQI greater than one implies a degraded ride in comparison to the baseline ride.

The first good quality evident about the index is that its complexity is independent of the number of degrees of freedom used in the model. As a matter of fact the computation time is the same for 25 degrees of freedom as for 2 degrees of freedom. Yet the RQI will show parametrically the tradeoff in degrees of freedom required to generate a meaningful load factor curve and will identify major contributors to the load factor curve.

Utilizing this concept, the RQI for the B-1 unaugmented vehicle was computed to separate the contributions of each elastic mode and the rigid body with the fully flexible vehicle as the baseline. Figure 2.3 shows the B-1 load factor curve with additional modes added into the load factor expression. Modes 1 and 3 are the major contributors to the total ride. A check in the mode shape data shows these two modes are primarily fuselage bending modes. Referring to Table 2.3 we can see the RQI associated with each mode. Clearly the index discriminates between major contributing modes and the less important ones. Note that a

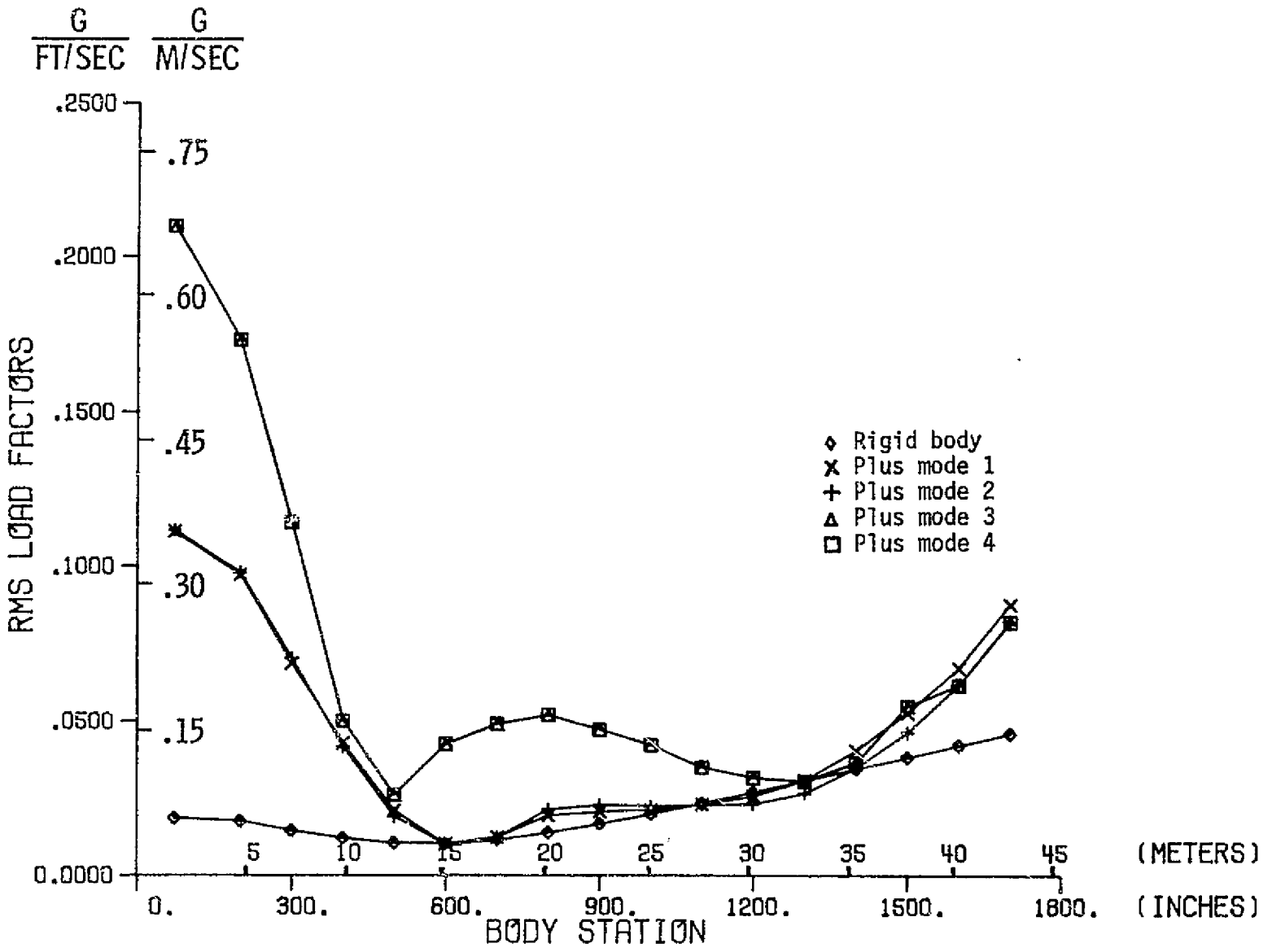

Figure 2.3 B-1 Unaugmented Vehicle Load Factors. Mach .85.

favorable effect has been gained by including the second elastic mode. It is barely recognizable on Figure 2.3 but is immediately evident with the RQI. This cancellation phenomenon will be discussed in chapters 5 and 6.

TABLE 2.3 B-1 Unaugmented Vehicle RQI

Load Factor Curve Includes:	RQI
Rigid body plus 4 elastic modes	1.0000
Rigid body plus 3 elastic modes	0.9997
Rigid body plus 2 elastic modes	0.5534
Rigid body plus 1 elastic mode	0.5643
Rigid body only	0.3406

Two more cases will be demonstrated concerning the RQI discrimination capability. The first case involves an obviously better ride. Figure 2.4 shows the B-52H load factor curve for pitch rate feedback with a gain of -.2 as compared to the unaugmented vehicle. Both curves include 4 symmetric elastic modes in the dynamic equations of motion and the load factor expressions. The destabilizing gain should, and actually does produce higher load factors.

The major discriminator in the RQI for this case is the area under the curve, E_i. The average, minimum, and maximum value discriminators all promote the lower curve but not with the degree of change seen by the area variable, E_i. The next example will show the metric's utility with intersecting curves.

In the cases where the areas under the load factor curves are nearly equal, some philosophy about RQ must be expressed by the manager. Throughout this work we will assume that uniform load factor values are better rides than highly sloped load factor curves with large minimum/maximum load factor differences. Consider Figure 2.5 for the B-52H relaxed static stability case. The handling qualities have been restored by a SAS. Which load factor curve is a better ride? Under the assumption at the beginning of this paragraph, the RSS ride looks worse.

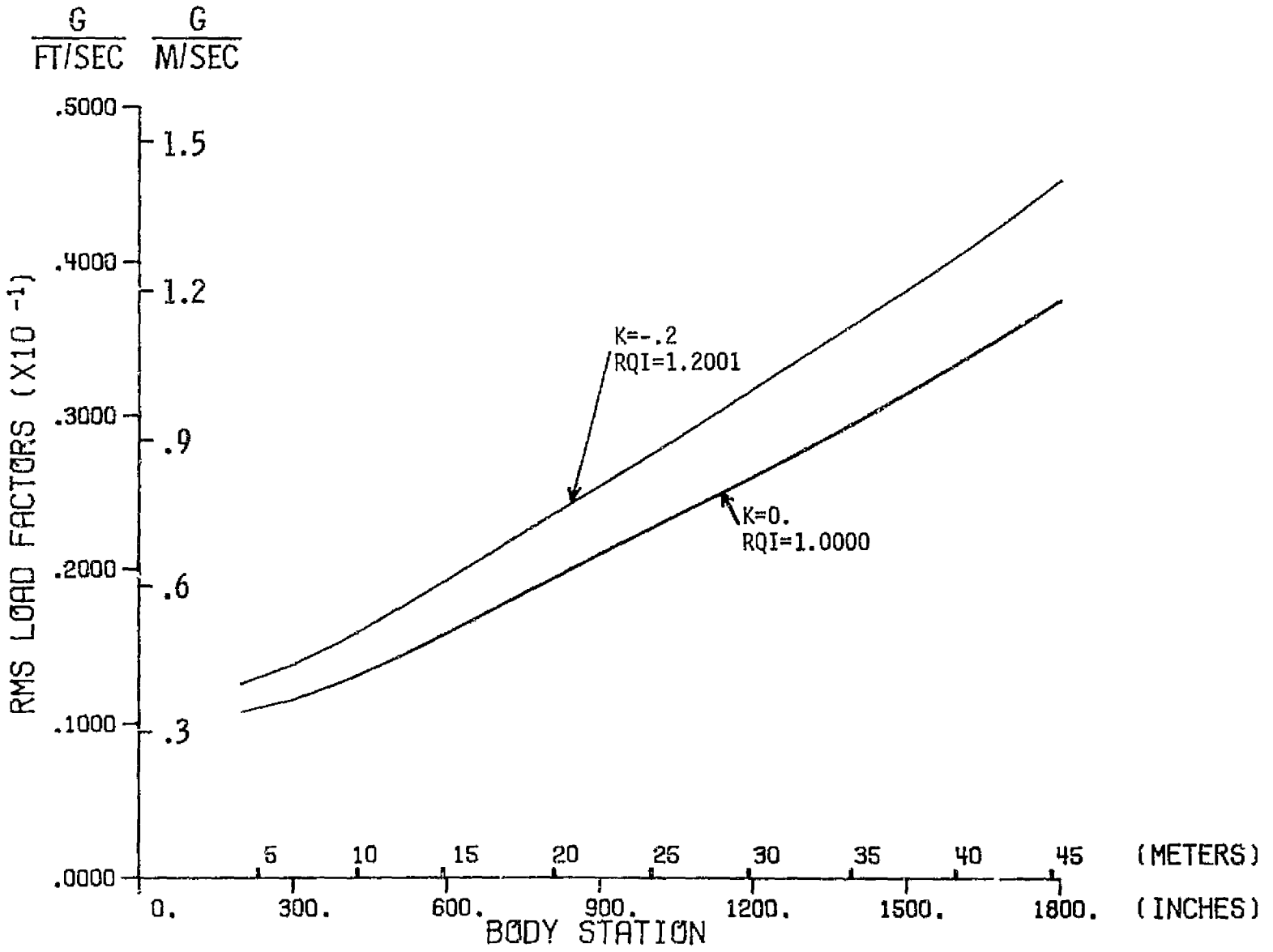

Figure 2.4 B-52H Pitch Rate Feedback RQI. Mach .55, Altitude 610 m (2000 ft).

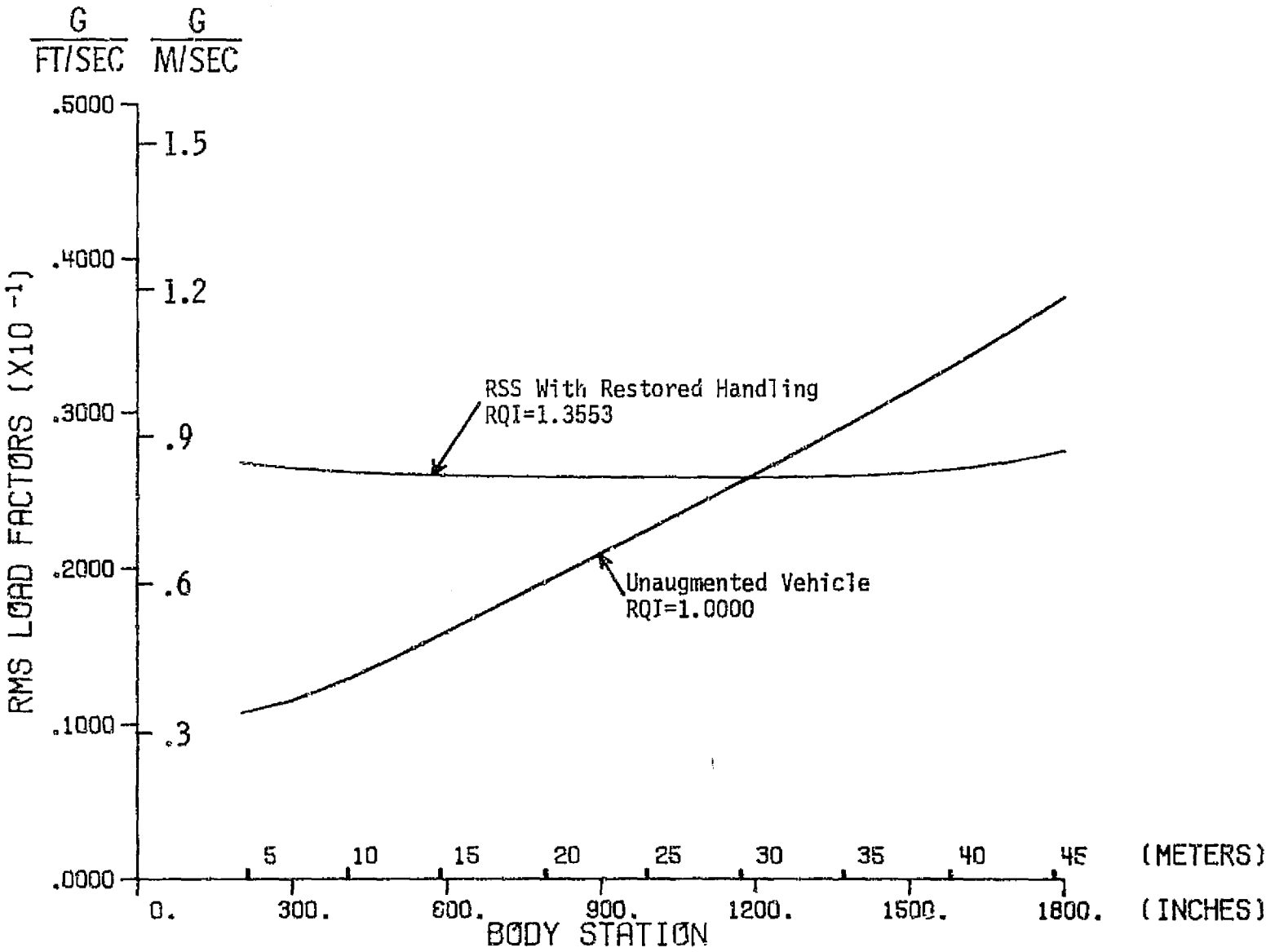

Figure 2.5 B-52H RQI Discrimination. Mach .55, Altitude 610 m (2000 ft).

Note that there is an order of magnitude scale factor difference between the B-1 and B-52H curves.

Note the RQI attached to each curve computed by equation 2.13. The major discriminators at work here counterbalance each other in the following way. The minimum value is worse. The maximum value is better. The total area under the curves is nearly the same but favors the unaugmented case. The average value favors the unaugmented case. The result is a worse ride for the RSS case according to the RQI. Certainly visual examination infers the same, but closer cases might not be as graphically discriminated.

Finally the obvious modification for the RQI is a weighting assigned by the design manager for particular effects. If the purpose of the designed vehicle is transportation of vibration sensitive cargo, then more weighting could be applied to the area under the curve and the maximum value discriminators. Alternatively, the acceleration at a particular station might be of interest and carefully adjusted because of highly sensitive equipment. The possibilities are unlimited depending on the manager's design problem and his philosophy. This index will be used to evaluate the B-52H and B-1 RQ in the remainder of this thesis. Instead of summarizing this chapter's contents the last section will discuss the utility of the RQI in a marketing context.

2.6 RQI Marketing Example

For this problem I propose an even simpler RQI than equation 2.13. Consider only the area under the load factor curve. It represents energy imparted to passengers, cargo, avionics, pilots, and equipment along the vehicle centerline. Suppose we wish to show the cost tradeoffs to a consumer airline board of executives for better passenger rides. The better ride costs more because of increased control requirements. But it might generate favorable advertising or selling points for their customers that would offset the initial direct cost and the lifetime costs.

First the executives need to determine what level of vibration is acceptable to their particular passenger market. They can easily calculate the equivalent of the RQI baseline figure.

The RQI can be computed according to formula 2.14:

$$RQI = \frac{E_i}{E_{BL}} \tag{2.14}$$

where: E_i the total area under the load factor curve for a particular control and handling quality.

E_{BL} the baseline energy computed by multiplying the human rms perception level (in g's/m/sec (g's/ft/sec)) times the fuselage length of the vehicle.

The RQI for marketing is now a weighted multiple of the human perception level accelerations. Of course any baseline could be used. Taking discrete jump values for control law complexity and linear multipliers for handling quality requirements within that control law, the cost function might look like 2.15:

$$\text{Cost}(\$) = \text{Control Law Complexity Value} + [RQI][HQ] \tag{2.15}$$

The control law complexity value in 2.15 is meant as an initial hardware cost for implementing the desired control philosophy. The RQI is defined in equation 2.14. The "HQ" function is envisioned as a dollar cost per RQI value. Basically this represents the cost of engineering development, interface, and testing problems which each control system must have resolved. It is necessarily a function of the amount of ride control required on the vehicle. Thus, the marketing experience of the manufacturers would probably give a reasonable initial definition for this costing variable.

Figure 2.6 shows a fictional example of what costing information might be available to the consumer airline's board. The constant dollar lines represent the initial hardware cost for different control law complexity. For example here we will assume that rate feedback hardware will cost $150,000 per vehicle. A modified state feedback system might cost $400,000 for initial hardware.

Once a type of control law is chosen, the maximum ability to reduce the RQI is set. The curves in Figure 2.6 would then represent

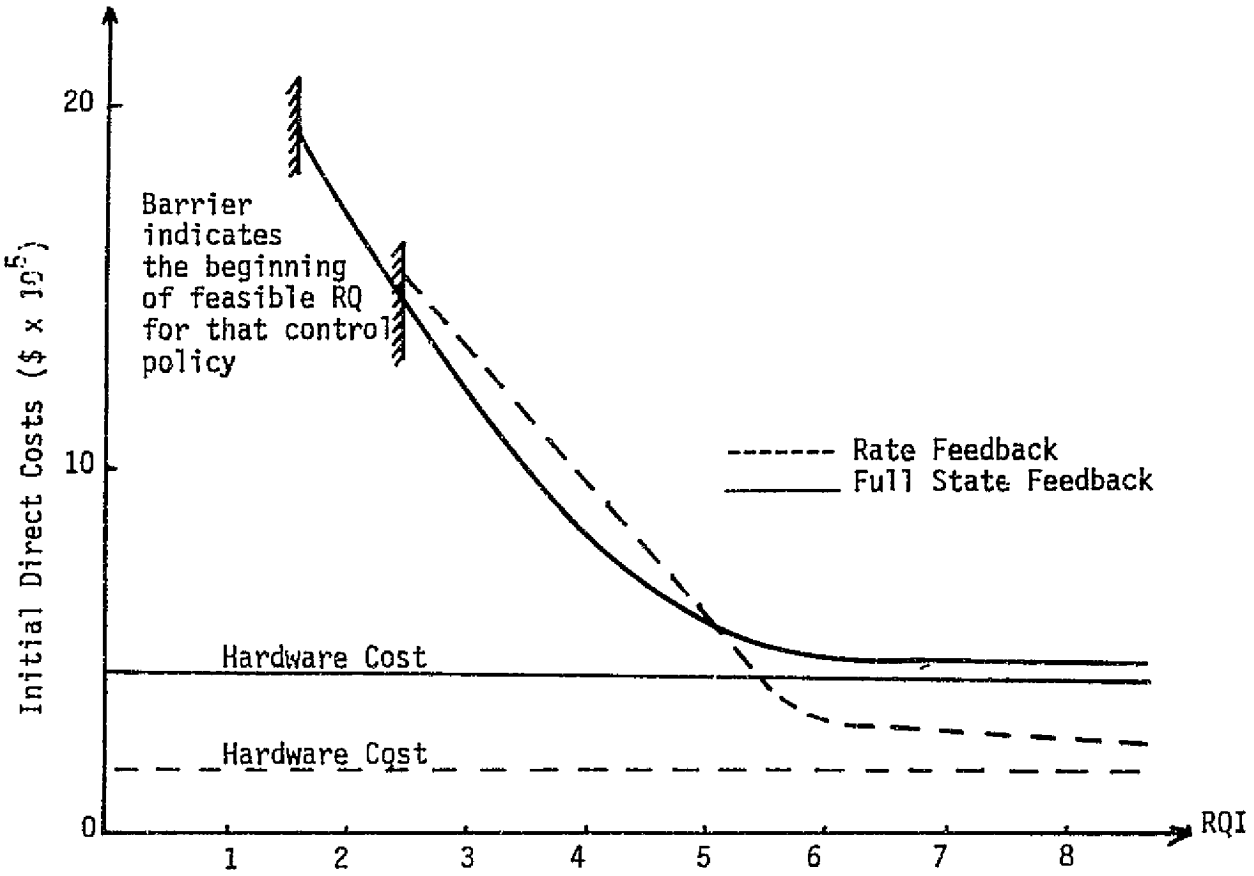

Figure 2.6 SAS Costs For Various Rides. Fictional Cost Curves (For Example Only).

the feasible RQ and its direct cost to the consumer airline. The utility of this representation depends on the board's comprehension of what rides their passengers are willing to buy.

Again, this scenario has been completely fictional. Chapter 3 will show that the RQ is not significantly affected by the type of control law. Chapter 4 will show that RQ is very sensitive to handling quality specifications. The "HQ" function in equation 2.15 is therefore closely related to the cost of developing certain handling qualities under all the other design constraints.

Finally, the marketing index might be adapted to a particular value appropriate to avionics maximum vibration levels. The possibilities are limitless. The design engineer and consumer managers would have a tradeoff tool to judge or delineate differences for the ride quality problem.

Chapter 3

RIDE QUALITY SENSITIVITY TO DIFFERENT CONTROL LAWS

3.1 Control Law Descriptions and Study Constraints.

The achievement of a specification for RQ is dependent on a thorough understanding of the effects of various contemporary control policies. There are wide ranging effects and advantages to be gained by increasing complexity for control laws. But the cost is not always justifiable. For an instance, rate feedback is used on many vehicles because it is easy to model, costs less to implement, and ultimately results in lower life-cycle maintenance requirements. A more complex control policy was introduced in the 1960's by D.T. Makers (reference 3) and is called "C-Star" (C*). The policy is a blend of pitch rate and plunge acceleration such that handling characteristics which pilots seem to favor can be maintained over larger ranges of steady state angle of attack. The design and implementation costs for C* are higher but the handling qualities are more acceptable over a wider range of flight conditions.

Is the RQ better for more complex control laws? Examination of this question requires several constraints and assumptions. First, the handling qualities of the short period longitudinal equations will be maintained as nearly equal as possible between the various control law test cases. Second the four elastic modes for both vehicles will be included in the parameterizations. Third, sensing of required physical output will be accomplished at the cg for cases where it is required. Admittedly this last constraint is certainly sub-optimal but our purpose is not to optimize the ride for a specific vehicle. Fourth, it is assumed that only major control surfaces, such as elevator, aileron, and rudder, are available for control in this model. This specifically

eliminates the B-1 Structural Mode Control System (SMCS) for our purposes. Again, the primary objective for this study does not include optimization of a particular aircraft's control system to provide good RQ. The results of this section must be considered in light of the above assumptions.

The control laws investigated include pitch rate, pitch rate/pitch attitude, C*, and full state feedback. Full state feedback is not currently used in aerospace vehicles as a physically realizable feedback law, but its exact pole placing capability insured "perfect" matching of controls for several cases in this part of the investigation.

3.2 Control Law Modeling.

The common starting point for all of the derivations is the state vector equation A.8. The states, matrices, and white noise are defined in the same manner as the Chapter 2 treatment of this 13th order system.

$$\dot{x} = Ax + Bu + Gn \tag{A.8}$$

The control u(t) will be elevator deflections for all cases in this thesis.

3.3 Pitch Rate Control

First for pitch rate we set $u = -Kx_6$, where $x_6 = \dot{\theta}$. In expanded form the pitch rate control looks like 3.1:

$$\dot{x} = \begin{bmatrix} a_{11} & \cdots & a_{15} & (a_{16} - KB_1) & a_{17} & \cdots & a_{1,13} \\ a_{21} & \cdots & a_{25} & (a_{26} - KB_2) & a_{27} & \cdots & a_{2,13} \\ \vdots & \cdots & \vdots & \vdots & \vdots & \cdots & \vdots \\ a_{10,1} & \cdots & a_{10,5} & (a_{10,6} - KB_{10}) & a_{10,7} & \cdots & a_{10,13} \\ 0 & \cdots & \cdots & \cdots & \cdots & \cdots & \begin{bmatrix}(3 \times 3) \\ A_g\end{bmatrix} \end{bmatrix} x + Gn \tag{3.1}$$

Selection of a gain value K results in a deterministic A* matrix which possesses certain coupled eigenvalues. Table 3.1 shows the gains, short period damping, and short period natural frequency for each case used on the study vehicles. The frequencies are shown in rad/sec. A reference case number will be shown in all the tables. Some cases were inconclusive or irrelevant for certain parts of this investigation. Therefore the tables will not be strictly sequenced according to case numbers. The four elastic mode free-free natural frequency and damping values remain the same as in Appendix A and are not listed in Table 3.1.

TABLE 3.1: Pitch Rate Feedback Parameterizations

B-52H CASE #	$\omega_{n_{SP}}$	ζ_{SP}	GAIN		ζ_{SP}	$\omega_{n_{SP}}$	B-1 CASE #
1	2.806	.5157	0.	0.	.4708	2.790	1
2	2.635	.4040	-.2	-.1	.2650	2.981	4
3	2.970	.6170	+.2	+.1	.6551	3.168	2
4	3.126	.7120	+.4	+.2	.8240	2.594	3

3.4 Pitch Rate/Pitch Attitude Control

Utilizing this same procedure the parameterization for pitch rate/pitch attitude was computed under the control equation 3.2. The artificial state x_0 was generated by adding the integral of $\dot{\theta}$ to the state system, making it 14th order.

$$u = -K_1 x_0 - K_2 x_6 \tag{3.2}$$

where K_1 Pitch attitude gain

K_2 Pitch rate gain

Table 3.2 shows the cases chosen for testing under this control law.

3.5 Blended Pitch Rate and Acceleration (C*)

This control philosophy is used mostly with fighter or maneuvering types of vehicles. However, the purpose here was to parameterize over common control laws and so it is included in the investigation.

TABLE 3.2: Pitch Rate/Pitch Attitude Parameterizations

B-52H CASE #	K_1	K_2	ζ_{SP}	$\omega_{n_{SP}}$
10	.25	-.2	.3590	2.754
11	.25	.5	.7230	3.272
12	.75	.6	.7060	3.497
13	.25	.1	.5280	2.982
14	.25	-.3	.2970	2.677
B-1 CASE #				
15	.1	0.	.4230	2.955
16	.1	.2	.7760	3.288
17	.3	.2	.6950	3.550
18	.4	.3	.8170	3.817

$$u = -K_1 a_z - K_2 \dot{\theta} \tag{3.3}$$

The values chosen for load factor evaluations are shown in Table 3.3. Since the cg plunge acceleration is approximately equal to $U(\dot{\theta} - \dot{\alpha})$, the form of equation 3.3 for implementation was actually equation 3.4:

$$u = K_1 U x_5 - (K_1 U + K_2) x_6 \tag{3.4}$$

where K_1 Acceleration gain
K_2 Pitch rate gain

3.6 Full State Feedback

In this procedure the roots of the desired characteristic polynomial were specified. Then the difference between the open and closed loop characteristic polynomial coefficients were computed. These values were transformed under the inverse of the phase variable canonical transformation matrix to find the physical state variable gain matrix, K.

TABLE 3.3: C* Parameterizations

B-52H CASE #	K_1	K_2	ζ_{SP}	$\omega_{n_{SP}}$
5	-.0005	0.	.3403	2.521
6	-.0005	.3	.5140	2.779
7	-.0001	0.	.4820	2.751
8	.0003	-.2	.5060	2.806
9	.0004	.5	.8560	3.402
B-1 CASE #				
5	-.0005	.4	.3220	2.483
6	-.0004	[illegible]	.3100	2.504
7	-.0004	.4	.5230	2.685
8	-.0004	.5	.7160	2.862
9	.0001	0.	.6410	3.013
10	.0001	.1	.8080	3.204
11	.0003	-.3	.4340	2.881
12	.0003	-.2	.6120	3.084
13	.0005	-.4	.5840	3.160
14	.0005	-.2	.8890	3.570

The procedure is mathematically outlined below. Beginning with the original state variable system:

$$\dot{x} = Ax + Bu + G\eta \qquad (A.8)$$

Delete the three gust state equations and rewrite the equation as 3.5:

$$\dot{x} = \bar{A}x + \bar{B}u + A_{gf}\, x_g \qquad (3.5)$$

where: $\bar{A}$ and $\bar{B}$ do not include the gust coefficients

A_{gf} is the aerodynamic gust force coefficients from A in A.8

x_g are the longitudinal gust states

Now we perform a similarity transformation on x such that $x = Ty$ or $y = T^{-1}x$.

Substituting in 3.5 yields

$$\dot{y} = T^{-1}A\,T\,y + T^{-1}B\,u + T^{-1}A_{gf}\,x_g \tag{3.6}$$

The matrix $[T^{-1}AT]$ is called the phase variable canonical form and has the expanded form:

$$[T^{-1}AT] = \begin{bmatrix} 0 & 1 & 0 & \cdots & 0 \\ 0 & 0 & 1 & 0 & \cdots & 0 \\ \vdots & & \ddots & \ddots & & \vdots \\ \vdots & & & \ddots & \ddots & \vdots \\ \vdots & & & & \ddots & 0 \\ 0 & \cdots & \cdots & \cdots & 0 & 1 \\ -d_0 & -d_1 & \cdots & \cdots & \cdots & -d_{n-1} \end{bmatrix} \tag{3.7}$$

The coefficients, d_i, relate to the characteristic equation of A as in 3.8:

$$|sI-A| = s^n + d_{n-1}s^{n-1} + \ldots + d_1 s + d_0 \tag{3.8}$$

The canonical form 3.7 provides an easy method for determination of the physical variable gain matrix, K.

Let the $|k_i|$ row vector be equal to the differences of the matched coefficients of the open and closed loop characteristic equations. Then $T^{-1}Bk$ is an nxn matrix which is null except the last row:

$$[T^{-1}Bk] = \begin{bmatrix} 0 & \cdots & 0 \\ \vdots & & \vdots \\ 0 & \cdots & 0 \\ k_0 & k_1 \cdots & k_{n-1} \end{bmatrix} \tag{3.9}$$

The closed loop characteristic equation coefficients are:

$$|sI-A^*| = s^n + e_{n-1}s^{n-1} + \ldots + e_1 s + e_0 \tag{3.10}$$

Therefore the $\lfloor k_i \rfloor$ matrix is related to the open and closed loop coefficients by: $e_i = d_i - k_i$. Substitution for $u = -Kx = -KTy$ yields:

$$[T^{-1}Bk_i] = [-T^{-1}BKT] \tag{3.11}$$

But, $[T^{-1}B]' = \lfloor 0 \ldots 0\ 1 \rfloor$ which implies:

$$K = \lfloor -k_i \rfloor T^{-1} \tag{3.12}$$

Hence with the characteristic equation coefficient differences known, the physical state gains K can be computed. The similarity transform T is computed using an algorithm suggested in reference 4. Given the control coefficient matrix B, the state coefficient matrix A, and the open loop characteristic equation coefficients, d_i, we compute T as follows:

Let $T = [t_1 \vdots t_2 \vdots \ldots \vdots t_n]$ where t_i are column vectors. Then

$$t_n = B$$

$$t_{i-1} = At_i + d_i B \qquad (i=n,n-1,\ldots,2) \tag{3.13}$$

A computational problem arose with the accuracy of the T matrix. Appendix C, section C.4 discusses the problem and the solution method used as a result.

The gains and associated short period damping and frequencies are logged in Table 3.4 for the B-52H and Table 3.5 for the B-1. All of the gains are reasonable in magnitude and in that sense represent physically realizable system values. Two exceptions to this statement are the B-1 cases #21 and #22. In these two cases a large elastic damping increase was imposed for investigative purposes. The high gains required were not unexpected nor were they intended as physically realizable.

3.7 Control Law Variation Results

For the cases where damping and natural frequency were nearly identical, the load factor curves were nearly identical. They were so close that numerical 4 digit load factor hardcopy had to be compared to find any differences. As a result the RQI was utilized on these cases and the results are compiled in Table 3.6.

TABLE 3.6: Control Law Parameterizations, B-52H

B-52H CASE #	Type Control	$\omega_{n_{SP}}$	ζ_{SP}	RQI
1	$\dot{\theta}$	2.806	.5157	1.0000
6	C*	2.779	.5140	0.9813
24	Full State	2.806	.5157	0.9991
12	$\theta/\dot{\theta}$	3.497	.7060	0.7992
31	Full State	3 400	.8175	0.8128

Cases 12 and 31 provide a reasonable implication that the same equivalence phenomena exists for $\theta/\dot{\theta}$ controls. In all cases shown the RQI difference is less than two percent. Appendix C, section 5 contains the load factor plots for cases 6 and 12 so that the reader may compare them to cases 1 and 31, respectively. Cases 1 and 24 in Table 3.6 are both for the bare airframe (no SAS), but the pitch rate state equation 3.1 was used for Case 1 and the full state formulation of equations 3.6, 3.7, and 3.9 used for Case 24. These served as check cases for the two formulations on identical dynamics.

TABLE 3.4: B-52H Full State Feedback Parameterizations

B-52H CASE #	$\omega_{n_{SP}}$	ζ_{SP}	K_1	K_2	K_3	K_4	K_5	K_6	K_7	K_8	K_9	K_{10}
24	2.806	.5157	0	0	0	0	0	0	0	0	0	0
25	2.806	.3250	-.004	.06	-.01	.02	-.34	.28	-.0006	-.007	.002	-.001
26	2.806	.8176	.006	-.09	.03	-.03	.54	-.44	.001	.01	-.002	.001
27*	2.806	.5157	-.005	.59	-1.4	-.01	.19	-.02	.001	-.08	.329	-.024
28*	2.806	.3250	-.01	.73	-1.73	-.85	-.14	.25	.009	-.08	.313	-.03
29*	2.806	.8176	.004	.38	-.85	-1.0	.71	-.45	.003	-.08	.35	-.02
30	3.000	.8176	.008	-.11	.03	-.03	.34	-.52	.001	.015	-.003	.002
31	3.400	.8175	.01	-.13	.04	-.04	-.14	-.68	.001	.022	-.003	.002

*Increased damping on elastic modes.

TABLE 3.5: B-1 Full State Feedback

B-1 CASE #	$\omega_{n_{SP}}$	ζ_{SP}	K_1	K_2	K_3	K_4	K_5	K_6	K_7	K_8	K_9	K_{10}
19	2.790	.4708	0	0	0	0	0	0	0	0	0	0
20	2.790	.4708	0	0	000	0	0	0	0	0	0	0
21*	2.790	.4707	-.01	-.16	-.19	659.	-1.04	-.17	-.002	.02	-.003	28.97
22*	2.790	.4707	-.02	-.06	-.24	894.6	-1.92	-.21	-.003	.03	-.002	27.43
23	2.790	.6551	-.0008	.003	.001	-1.73	.06	-.08	-.00003	.0001	-.00007	.23
24	2.980	.6131	-.0007	.003	.001	-1.72	-.02	-.08	-.00002	.0001	-.00007	.22
25	.2296	-0-	-.002	.008	.001	-.01	.66	-.16	.0001	.0002	-.000036	.000096

*Increased damping on 1st and 3rd elastic modes.

Chapter 4

RIDE QUALITY SENSITIVITY TO HANDLING CHARACTERISTICS

4.1 Handling Quality Specifications

The recognized compendium of handling quality information is reference 16, MIL-F-8785B (ASG) "Military Specification - Flying Qualities of Piloted Airplanes". This document divides the vehicle handling quality design specifications into the following:

Kind of airplane - Class

Job to be done - Category of Flight Phase

Degree of job accomplishment - Level

For the study vehicles used herein the following definitions will apply:

Class III - Heavy bomber

Flight Phase - Category B (CR-cruise)

Level 1 - Qualities are clearly adequate for the mission flight phase.

Short period damping and natural frequency are very important to the pilot's perception of response. If the damping is too high, then the vehicle will be sluggish and slow to respond to the pilot inputs. If the damping is too low, the pilot will overcontrol the system because it reacts too quickly and will overshoot his desired output. This can develop into a "PIO" or pilot induced oscillation. As a result, the MIL-F-8785B short period damping limits are in the range $.3 \leq \zeta_{SP} \leq 2.0$ for the B-1 and B-52H types of vehicles.

The short period frequency is also important in the pilot's perception of a "good flying" vehicle. As the frequency decreases, the pilot must introduce a phase lead into his commanded inputs to maintain precise control. At the upper end of the acceptable short period frequency spectrum the pilot experiences abrupt control requirements to maintain precise vehicle attitudes.

Figure 4.1 shows the appropriate frequency requirements for the B-1 and B-52H. The unaugmented vehicle values are shown appropriately placed within the level 1 acceptable boundaries. This graph is taken from the reference 16 section on longitudinal specifications.

4.2 Variations in Handling Qualities

In each control law described in chapter 3 the short period frequency and damping was adjusted within the boundaries specified above. Lists of the variations induced on each vehicle are outlined in Table 4.1 for the B-52H and Table 4.2 for the B-1. Certain cases are again not included in the lists because they did not apply to this investigation. Tables 4.3 and 4.4 list the data according to decreasing RQI. The expected trend is substantiated by these cases. Increasing damping and increasing frequency generate better rides.

To further verify these expected trends full state feedback was used to increase the short period frequency while maintaining the same damping. Figure 4.2 shows the apropos change in load factor for the increased frequencies. The ride is definitely improved with increased frequency.

The trend for damping is the same. Table 4.5 shows the data for the B-52H sorted with respect to damping. Table 4.6 shows the same sorting for the B-1. Increased rigid body damping generally produces a better RQI.

4.3 Ride Quality for Increased Damping of Elastic Modes

On the B-52H a full state feedback program was implemented to find the effect of increasing the coupled damping on the elastic modes to a .1 minimum value. Table 4.7 shows the changes involved. The elastic frequencies were held constant at the bare airframe coupled value throughout these cases.

Figure 4.3 shows the percent change in ride experienced for increased elastic damping for the two short period cases of Table 4.7. At this juncture the expected trend is reversed. Increased damping on the elastic modes produced an eight to ten percent worse load factor at most stations than the same case without increased elastic damping.

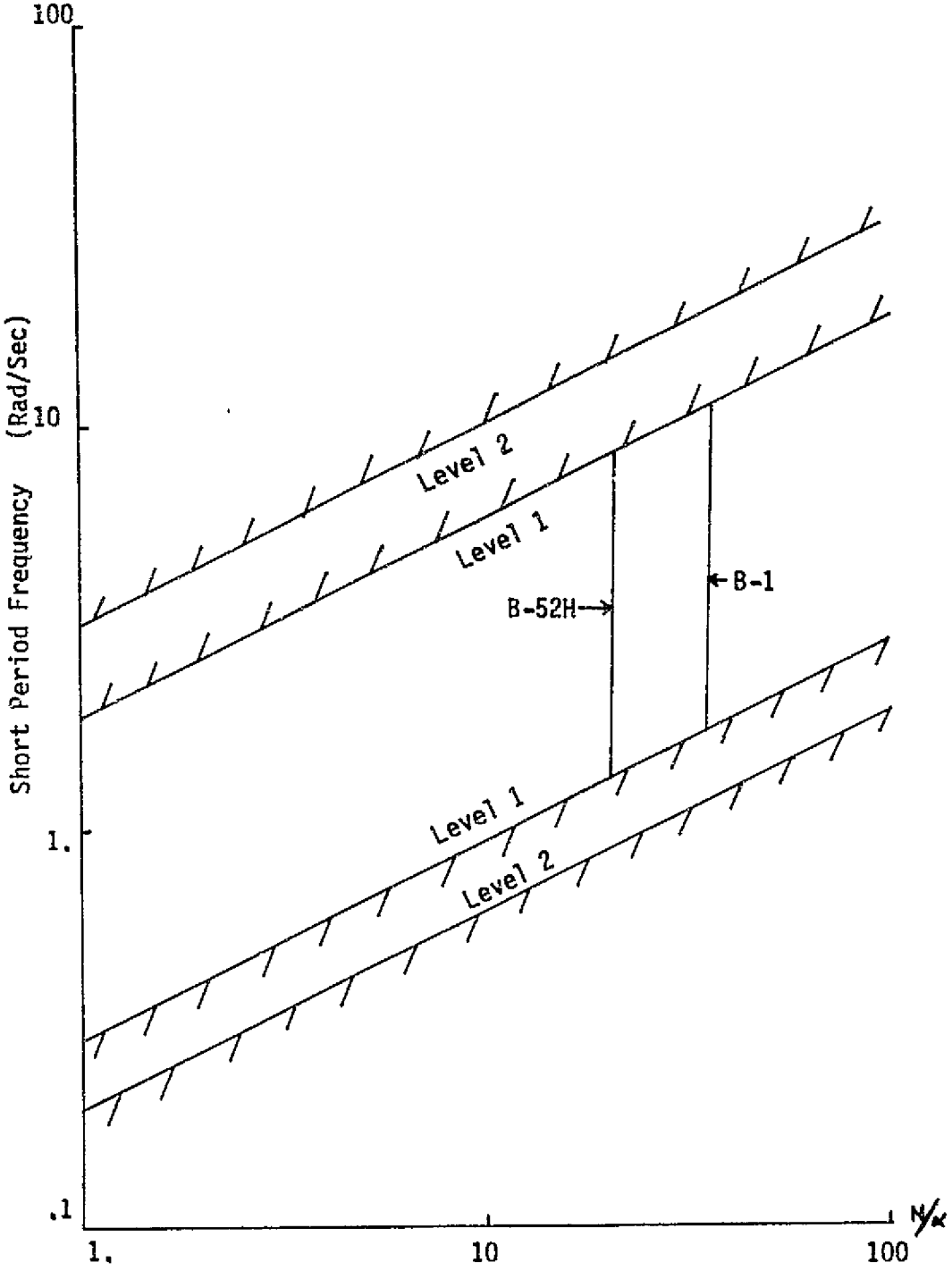

Figure 4.1 Short Period Frequency Requirements

TABLE 4.1: B-52H Handling Quality Variations

B-52H CASE #	SAS TYPE	ζ_{SP}	$\omega_{n_{SP}}$
1	$\dot{\theta}$	.5157	2.806
2	$\dot{\theta}$	.4040	2.635
3	$\dot{\theta}$	.6170	2.970
4	$\dot{\theta}$	.7120	3.126
5	C*	.3403	2.521
6	C*	.5140	2.779
7	C*	.4820	2.751
8	C*	.5060	2.806
9	C*	.8560	3.402
10	$\theta/\dot{\theta}$	.3590	2.754
11	$\theta/\dot{\theta}$	.7230	3.272
12	$\theta/\dot{\theta}$	.7060	3.497
13	$\theta/\dot{\theta}$	.5280	2.982
14	$\theta/\dot{\theta}$	.2970	2.677
24	Full State	.5157	2.806
25	Full State	.3250	2.806
26	Full State	.8176	2.806
27	Full State	.5157	2.806
28	Full State	.3250	2.806
29	Full State	.8176	2.806
30	Full State	.8176	3.000
31	Full State	.8175	3.400

TABLE 4.2: B-1 Handling Quality Variations

B-1 CASE #	SAS TYPE	ζ_{SP}	$\omega_{n_{SP}}$
1	$\dot{\theta}$	.4708	2.790
2	$\dot{\theta}$	.6551	2.981
3	$\dot{\theta}$	.8240	3.168
4	$\dot{\theta}$	.2650	2.594
5	C*	.3220	2.483
6	C*	.3100	2.504
7	C*	.5230	2.685
8	C*	.7160	2.862
9	C*	.6140	3.013
10	C*	.8080	3.204
11	C*	.4340	2.881
12	C*	.6120	3.084
13	C*	.5840	3.160
14	C*	.8890	3.570
15	$\theta/\dot{\theta}$	.4230	2.955
16	$\theta/\dot{\theta}$	.7660	3.288
17	$\theta/\dot{\theta}$	.6950	3.550
18	$\theta/\dot{\theta}$	.8170	3.817
19	Full State	.4716	2.790
20	Full State	.4707	2.790
21	Full State	.4707	2.790
22	Full State	.4707	2.790
23	Full State	.6551	2.790
24	Full State	.6132	2.980
34	Full State	.8240	3.168
35	Full State	.4708	2.790

TABLE 4.3: B-52H RQI Sorting Results

B-52H CASE #	RQI	DAMPING	NATURAL FREQUENCY
5	1.36964	.3403	2.521
14+	1.30822	.2970	2.677
28†	1.23552	.3250	2.806
29†	1.20517	.8176	2.806
2	1.20014	.4040	2.635
25	1.18949	.3250	2.806
10	1.14014	.3590	2.754
26	1.09571	.5157	2.806
27	1.08706	.5157	2.806
7	1.04233	.4820	2.751
8	1.02555	.5060	2.806
1	1.00000	.5157	2.806
6	.98127	.5140	2.779
30	.95562	.8176	3.000
3	.90211	.6170	2.970
13	.89950	.5280	2.982
4	.85491	.7120	3.126
9*	.84659	.8560	3.402
11	.81461	.7230	3.272
31	.81285	.8176	3.400
12+	.79921	.7060	3.497

This case does not follow the general trend as it was an investigation into stabilizing versus destabilizing gain effects for C feedback.

†Elastic mode suppression cases which do not follow the trend and will be discussed separately.

+These cases are included in the Appendix C, section C.5 plots.

TABLE 4.4: B-1 RQI Sorting Results

B-1 CASE #	RQI	DAMPING	NATURAL FREQUENCY
22†	5.66966	.4707	2.790
21†	5.61414	.4707	2.790
4+	1.06240	.2650	2.594
11	1.04007	.4340	2.881
13*	1.03435	.5840	3.160
6*	1.02579	.3100	2.504
5*	1.02025	.3220	2.483
15	1.00105	.4230	2.955
12*	1.00095	.6120	3.084
35	1.00045	.4708	2.790
1	1.00000	.4708	2.790
20	.99986	.4707	2.790
19	.99985	.4716	2.790
24	.97706	.6132	2.980
9	.97535	.6410	3.013
23	.97443	.6551	2.790
2	.96498	.6551	2.981
34	.96300	.8240	3.168
10	.95037	.8080	3.204
3	.94063	.8240	3.168
17	.94061	.6950	3.550
16	.93706	.7760	3.288
8	.93601	.7160	2.862
18+	.92292	.8170	3.817

*Cases involve stabilizing vs destabilizing gain effects.

†Elastic mode suppression cases.

+These cases are shown as load factor plots in Appendix C, section C.5.

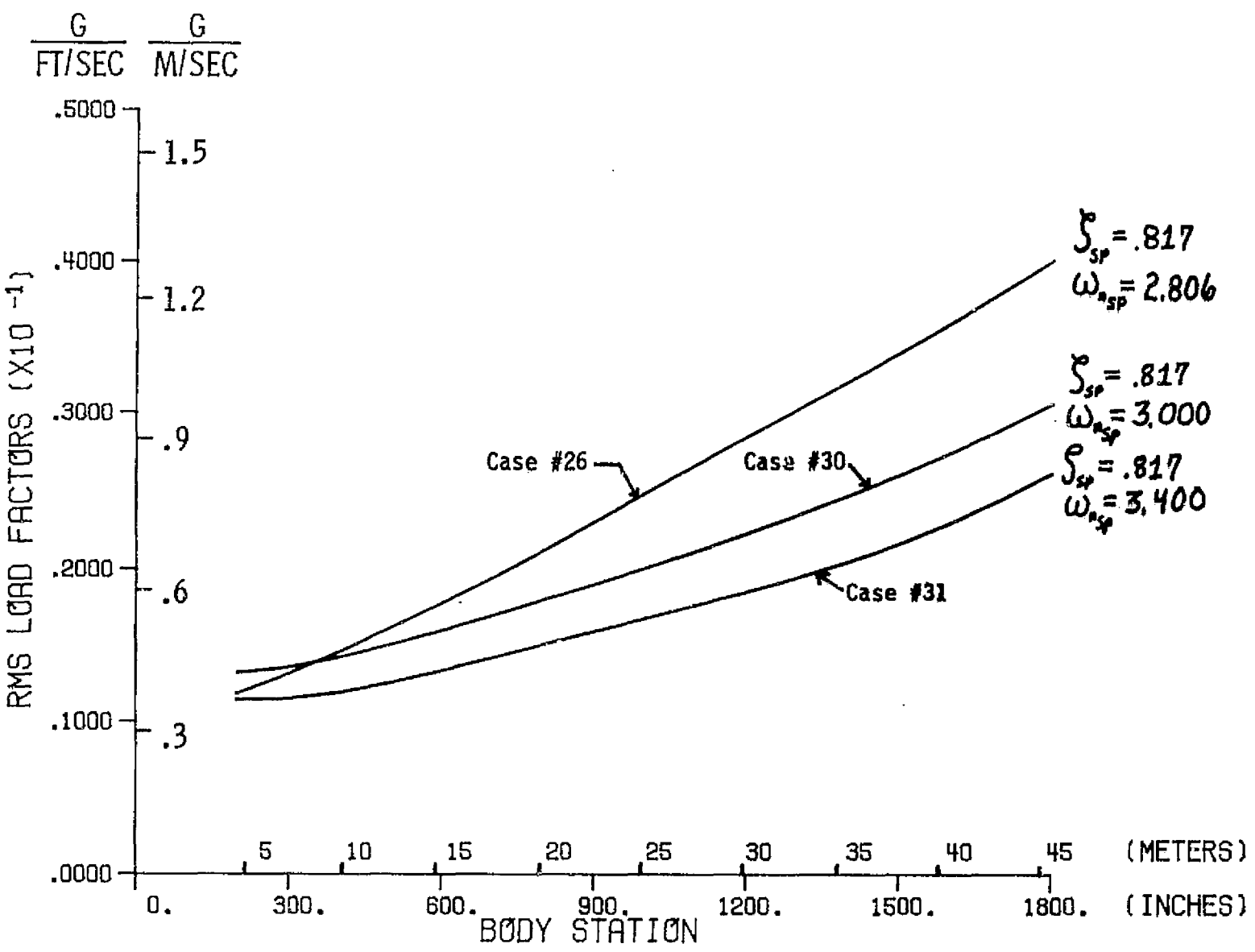

Figure 4.2 B-52H, Effect of Increased Natural Frequency. Mach .55, Altitude 610 m (2000 ft).

TABLE 4.5: B-52H RQI Sorted By Damping Value

B-52H CASE #	RQI	DAMPING	NATURAL FREQUENCY
14	1.3082	.2970	2.677
25	1.1895	.3250	2.806
28	1.2355	.3250	2.806
5	1.3696	.3403	2.521
10	1.1401	.3590	2.754
2	1.2001	.4040	2.635
7	1.0423	.4830	2.751
8	1.0256	.5060	2.806
6	.9813	.5140	2.779
27	1.0877	.5157	2.806
1	1.0000	.5157	2.806
13	.8995	.5280	2.982
3	.9021	.6170	2.970
12	.7992	.7060	3.497
4	.8549	.7120	3.126
11	.8146	.7230	3.272
31	.8128	.8176	3.400
30	.9556	.8176	3.000
29	1.2052	.8176	2.806
26	1.0957	.8176	2.806
9	.8466	.8560	3.402

TABLE 4.6: B-1 RQI Sorted By Damping Value

B-1 CASE #	RQI	DAMPING	NATURAL FREQUENCY
4	1.0624	.2650	2.594
6	1.0258	.3100	2.504
5	1.0202	.3220	2.483
15	1.0011	.4230	2.955
11	1.0401	.4340	2.881
21	5.6141	.4707	2.790
20	.9999	.4707	2.790
22	5.6697	.4707	2.790
35	1.0004	.4708	2.790
1	1.0000	.4708	2.790
19	.9998	.4716	2.790
13	1.0344	.5840	3.160
12	1.0009	.6120	3.084
24	.9771	.6132	2.980
9	.9754	.6410	3.013
2	.9649	.6551	2.981
23	.9744	.6551	2.790
17	.9406	.6950	3.550
8	.9360	.7160	2.862
16	.9370	.7760	3.288
10	.9504	.8080	3.204
18	.9229	.8170	3.817
34	.9630	.8240	3.168
3	.9406	.8240	3.168

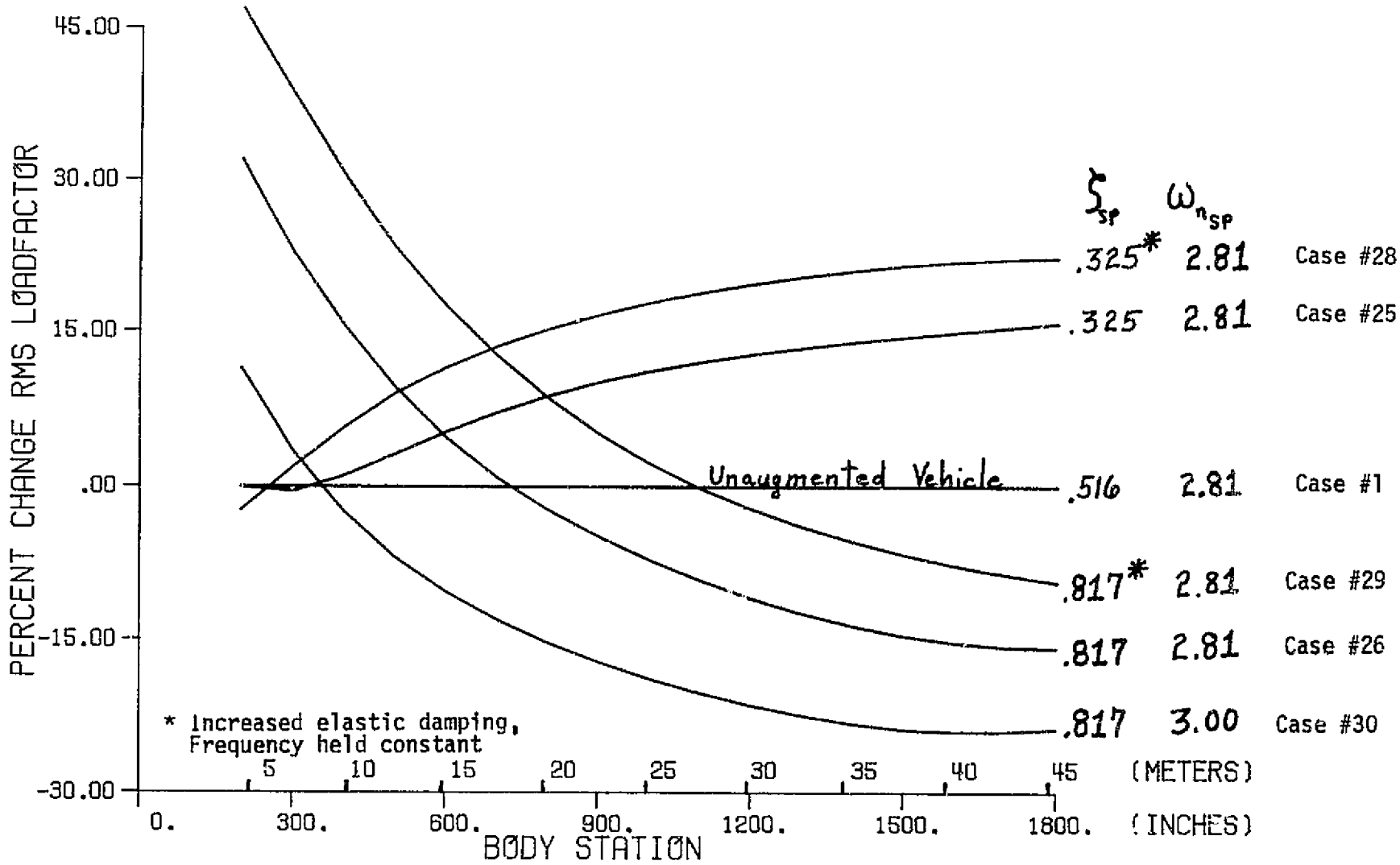

Figure 4.3 B-52H Full State Elastic Damping Changes. Mach .55, Altitude 610 m (2000 ft).

TABLE 4.7: B-52H Damping Changes for Elastic Modes

B-52H CASE #	SHORT PERIOD FREQUENCY	DAMPING SHORT PERIOD	MODE 1	MODE 2	MODE 3	MODE 4	RQI
25	2.806	.3250	.16	.08	.10	.06	1.189
26	2.806	.8176	.16	.08	.01	.06	1.095
28	2.806	.3250	.16	.10	.10	.10	1.230
29	2.806	.8176	.16	.10	.10	.10	1.200

This RQI trend reversal can be explained by the fact that the RMS elevator deflections were higher for the increased elastic mode damping cases. A check of the contributions to the load factor values showed that the elastic modes were damped more and actually contributed less to the overall ride. However, the rigid body RMS levels increased as a penalty and produced the degraded ride. A similar set of cases was run on the B-1 with identical results. This phenomenon deserves more research attention. There may be fatigue and/or RQ tradeoffs that would enhance structural life by useful cancellation of ride contributions due to elastic interactions.

Cases #21 and #22 in the B-1 parameterizations represent arbitrarily chosen increases in the coupled elastic damping values. The effect noted on the B-52H is much more pronounced on the B-1. Table 4.8 shows the B-1 damping change parameters and lists the RQI associated with each case.

TABLE 4.8: B-1 Damping Changes for Elastic Modes

B-1 CASE #	SHORT PERIOD FREQUENCY	DAMPING SHORT PERIOD	MODE 1	MODE 2	MODE 3	MODE 4	RQI
1	2.790	.4708	.047	.022	.009	.199	1.00
21	2.790	.4708	.100	.022	.090	.199	5.61
22	2.790	.4708	.200	.022	.100	.199	5.66

Again the increased rigid body accelerations far outweighed any gain in ride supplied by increased damping of the elastic modes. Furthermore the coupling with the elastic modes from the increased rigid body ride actually destroyed the favorable damping effect in the elastic contributions to the load factors. The rigid body load factor increased by a factor of ten when Case #1 was compared to Case #21.

RQ relationships to the short period handling qualities are very important. The investigation has shown that increased damping and/or frequency have produced generally favorable effects on the ride. Attempts to damp elastic modes using the primary elevator control resulted in degraded RQ because of the increased rigid body accelerations introduced.

Chapter 5

RIDE QUALITY SENSITIVITY TO RELAXED STATIC STABILITY

5.1 Aircraft Static Stability

The definition of longitudinal static stability can be related to a pitch stiffness quality as in Etkin's book, reference 5. If a vehicle is disturbed from an equilibrium angle of attack in a positive (nose up) direction, the total moment generated, $M_\alpha \Delta\alpha$, is negative and thus tends to return the vehicle to equilibrium. This case represents positive static stability. Figure 5.1 gives a pictorial representation of the forces and moments involved. The pitching moment is really a function of the stability derivative C_{m_α}, where $M_\alpha = \frac{\rho S U^2 c}{2I_y} C_{m_\alpha}$. All stability derivatives used in this study are defined in consonance with reference 6. A summary of the stability derivatives used in this chapter is given in the symbols listing at the front of this thesis.

Vehicles have traditionally been designed with positive static stability and cargo loading restrictions which maintain a minimum degree of longitudinal stability. Vehicles then need varying amounts of lift generated by the horizontal stabilizer to maintain cruise condition level flight. This results in a drag penalty that all vehicles in cruise conditions have had to accept to date. If, however, we were to modify the position of the center of gravity and the wing-body aerodynamic center such that $C_{m_\alpha} \to 0$, then less lift would be required to offset the moment due to the wing-body combination. Only a small lift, if any, would be required from the horizontal tail. This reduces the tail drag and results in better cruise efficiency. Increased cruise efficiency begets fuel economy. As fuel prices rise and availability declines, RSS will therefore be required as a design point on future vehicles.

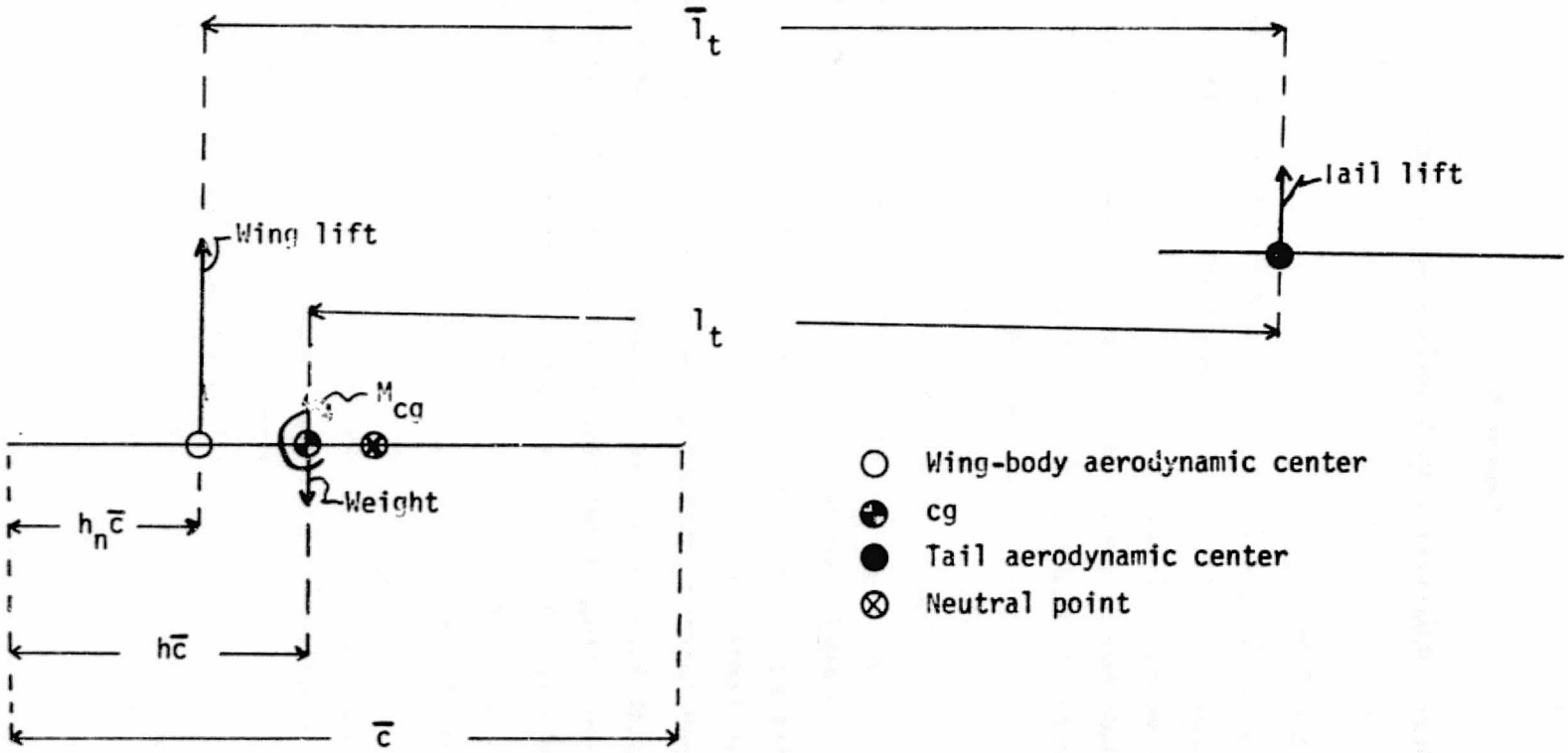

Figure 5.1 Longitudinal Stability Diagram; Major Parameters

5.2 Relaxed Static Stability

RSS refers to the relaxation of pitch stability requirements. The resulting fuel economy is one factor that new generation vehicles will have to incorporate in order that they remain competitive or even practical.

RSS can be implemented in several ways. First the tail surface area can be reduced. This decreases the moment restoring force and has the artificial effect of moving the neutral point toward the cg. Its value is purely theoretical. Second the center of gravity can be artificially moved toward the tail by fuel or cargo management. This method could be used on present vehicles. Lastly the engines and other major structural members of preliminary designs may be repositioned for better performance. Preliminary design RSS offers the most efficient implementation in my opinion. Any of these implementations may result in a neutral or statically unstable vehicle. The first two methods represent the techniques that will be used in this study.

RSS is basically a rigid body phenomenon, so only the short period equations for the rigid vehicle will be used to derive the "relaxed conditions". More elaborate models are possible using a variation of the technique developed by Swaim and Fullman in reference 12.

5.3 Equations of Motion in Stability Derivative Format

The time domain, short period, longitudinal equations of motion for rigid vehicles are given in 5.1:

$$\begin{aligned} \dot{w} - Z_w w - U\dot{\theta} &= Z_{\delta_e}\delta_e + Z_{\dot{w}}\dot{w}_g \\ -M_{\dot{w}}\dot{w} - M_w w - M_q\dot{\theta} + \ddot{\theta} &= M_{\delta_e}\delta_e + M_{\dot{w}}\dot{w}_g + \frac{M_q}{U}\dot{w}_g + M_w w_g \end{aligned} \tag{5.1}$$

where $w(t)$ Perturbation plunge velocity, positive in positive z axis direction

$w_g(t)$ Gust velocity, positive in negative z axis direction

$\theta(t)$ Perturbation pitch angle, measured from the x-y plane, positive nose up

δ_e Elevator deflection in radians, negative in B-1 and B-52 data for nose up changes

If we let $w = U\alpha$ and solve for accelerations on the left hand side, then 5.2 results:

$$\begin{bmatrix} U & 0 \\ -M_{\dot{w}}U & 1 \end{bmatrix} \begin{bmatrix} \dot{\alpha} \\ \ddot{\theta} \end{bmatrix} = \begin{bmatrix} Z_w U & U \\ M_w U & M_q \end{bmatrix} \begin{bmatrix} \alpha \\ \dot{\theta} \end{bmatrix} + \begin{bmatrix} Z_{\delta_e} & Z_w U & 0 \\ M_{\delta_e} & M_w U & M_{\dot{w}}U + M_q \end{bmatrix} \begin{bmatrix} \delta_e \\ \alpha_g \\ \dot{\alpha}_g \end{bmatrix} \tag{5.2}$$

Solving for $[\dot{\alpha}, \ddot{\theta}]'$ on the left hand side and noting that $q_g = \dot{\alpha}_g$ we get 5.3:

$$\begin{bmatrix} \dot{\alpha} \\ \ddot{\theta} \end{bmatrix} = \begin{bmatrix} Z_w & 1 \\ U(M_{\dot{w}}Z_w + M_w) & (UM_{\dot{w}} + M_q) \end{bmatrix} \begin{bmatrix} \alpha \\ \dot{\theta} \end{bmatrix} + \begin{bmatrix} Z_{\delta_e}/U & Z_w & 0 \\ (M_{\dot{w}}Z_{\delta_e} + M_{\delta_e}) & U(M_{\dot{w}}Z_w + M_w) & M_{\dot{w}}U + M_q \end{bmatrix} \begin{bmatrix} \delta_e \\ \alpha_g \\ q_g \end{bmatrix} \tag{5.3}$$

Equation 5.3 is the familiar control form 5.4:

$$\dot{x} = Ax + Bu + A_g x_g \tag{5.4}$$

The numerical values for all of these coefficient matrices are known in the B-1 and B-52H equations. From 5.3 it is easy to deduce that C_{L_α}, C_D, C_{m_α}, $C_{L_{\dot{\alpha}}}$, $C_{m_{\dot{\alpha}}}$, C_{m_q}, C_{L_q}, $C_{L_{\delta_e}}$, and $C_{m_{\delta_e}}$ are the stability derivative coefficients to be considered under RSS. Matching the appropriate coefficient combinations to the numerical equations of motion, and assuming that Z_w remains constant, we can generate the basic values for all of these coefficients. In preliminary design, the aerodynamics group would provide estimation for these derivatives after the planform and type of airfoil were established. Generation of the coefficients as described above was required in this work because the data did not include these numbers.

5.4 Relaxed Static Stability Effects on Stability Derivatives

How do these terms vary as tail volume coefficient or cg are changed to induce RSS? To keep the analytics tractable in the investigation, it is assumed that the vehicle will maintain the same lift

coefficient, weight, and cruise conditions. These assumptions are reasonable considering the accuracy of the original data. They are also reasonable if changes in the tail surface area or cg position are used that do not significantly alter the overall vehicle performance.

USAF DATCOM (reference 7) descriptions of the stability derivatives were used to generate the computerized equations of motion for the RSS cases. Table 5.1 lists the stability term equations for the B-52H. Table 5.2 has the B-1 stability coefficient changes. Recalling equation 5.3, it is seen that the baseline or "unrelaxed" values of Z_w and M_q are explicitly specified by the actual vehicle equations of motion. The remaining derivative values can be found by simultaneous solution of the matched coefficient equations. These values can be subjected to artificial RSS implementation, and by reversing the above procedure, a new set of equations of motion can be derived.

TABLE 5.1: B-52H RSS Stability Derivatives

$$M_w = 8.365 \times 10^{-3} - 4.655 \times 10^{7}[S_t][F_{cg}]$$

$$M_{\dot{w}} = -4.150 \times 10^{-3} - 2.768 \times 10^{-10}[S_t][F_{cg}]^2$$

$$M_q = 4.217 - 6.915 \times 10^{-7}[S_t][F_{cg}]^2$$

$$F_{cg} = 66.55 - [x_{cg} - .25][22.96]$$

$$Z_{\delta_e} = -3.756 \times 10^{-2}[S_t]$$

$$M_{\delta_e} = -16.058 - 1.228 \times 10^{-3}[S_t] + [x_{cg} + .856][12.129 - 4.239 \times 10^{-4}(S_t)]$$

$$Z_w = -1.352$$

Note: S_t is tail planform surface area

x_{cg} is the cg position from the wing leading edge normalized by the mean aerodynamic chord

Insufficient data was available in the Rockwell International documents (reference 15) to completely specify the derivatives for the B-1 from the equations of motion as given. As an example, the tail lift coefficient derivative with respect to alpha was assumed to be the nominal 2π value because it was not specified in the Rockwell document. This assumption was not critical in the study since it did not affect trend information except as a linear scaling factor. However, any actual design implementation of this technique would require the specification of this derivative.

TABLE 5.2: B-1 RSS Stability Derivative Coefficients

$$[C_{L_\alpha} + C_D] = 3.905$$

$$C_{m_\alpha} = 3.588 - 2.164 \times 10^{-4}[S_t][F_{cg}]$$

$$C_{m_{\dot{\alpha}}} = 6.288 - 1.611 \times 10^{-5}[S_t][F_{cg}]^2$$

$$C_{m_q} = 23.045 - 5.479 \times 10^{-5}[S_t][F_{cg}]^2$$

$$C_{N_{\delta_e}} = 1.895 \times 10^{-3}[S_t]$$

$$C_{m_{\delta_e}} = -2.528 - [5.462 \times 10^{-4} - (x_{cg}-.25)(15.33)][S_t] + 6.148 \times 10^{-2}(x_{cg}-.25)15.33$$

$$F_{cg} = 46.45 - (x_{cg} - .25)(15.33)$$

Note: S_t and x_{cg} are defined as in Table 5.1

5.5 Relaxed Static Stability Rigid Body Only Effects

Using the same algorithm for RQ, but rigid body 2 degree of freedom information only, a number of load factor plots were run for the B-52H. Figure 5.2 shows the B-52H results for decreasing static stability. Note the RQ effect that the pitch acceleration term is contributing less as the cg moves closer to the neutral point. Finally, at neutral stability, the only acceleration effect is the vertical acceleration generated by the cg movement.

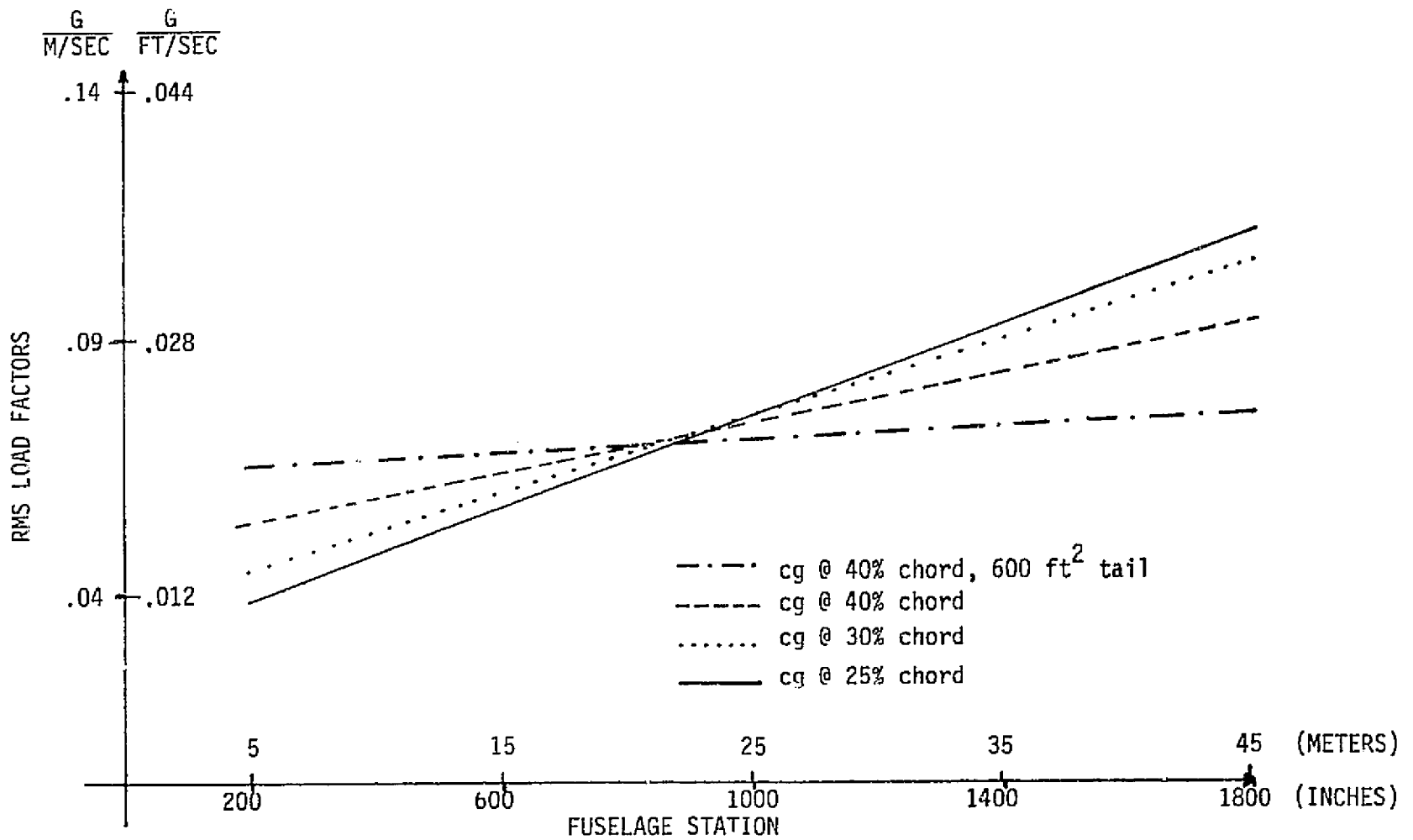

Figure 5.2 B-52H RSS, Rigid Body Only, No Elastic Dynamics.

5.6 Relaxed Static Stability With Restored Handling Qualities

For the first time in this study the significant difference between the elastic properties of the B-1 and B-52H will affect the outcome. Figure 5.3 shows the B-52H load factor curves for the rigid body plus 4 mode case and for the rigid body only. Even at the lower end of the curve, the elastic contribution to the ride is a maximum of 15%. Figure 5.4 shows the same unaugmented situation for the B-1, however the rigid body contribution is now the minor one. To be more exact, at body station 72 the rigid body contribution to ride is only 5% of the total B-1 ride. At other points on the fuselage the rigid body contribution is higher. Yet, the net effect is very little rigid body contribution to the overall ride on the B-1 for this flight condition.

The RSS vehicle equations of motion were augmented by full state feedback systems to restore the original unaugmented airframe handling characteristics for both vehicles. The resulting load factor curves were computed and compared to the bare airframe load factors.

Table 5.3 shows the RQI for each case and its associated data. In general the restored handling characteristics generated worse ride conditions because of the elevator activation required and its effect on the rigid body dynamics. Case #33 deserves special attention. The cg was 3.4 feet further aft in this case. The restored handling ride was actually better than the bare airframe ride as shown by the RQI. Figure 5.5 shows the Case #33 rigid and rigid plus four modes load factor curves in comparison to the bare airframe vehicle. Note in the figure the four modes and the rigid body have favorably interacted because the fully flexible load factor curve is lower in several areas. This favorable interaction has been prophesied and discussed in the literature but no practical technique is yet available for utilizing it. The favorable ride effects near the tail are due to decreased moment arm effects in the moment equation. For a fairly rigid fuselage, RSS with restored handling characteristics generally degraded the B-52H ride.

One phenomena on the less elastic B-52H went unnoticed but proved to be important on the B-1. As the static stability is reduced on the B-1 the rigid body dynamic effect produced by the elastic modes is

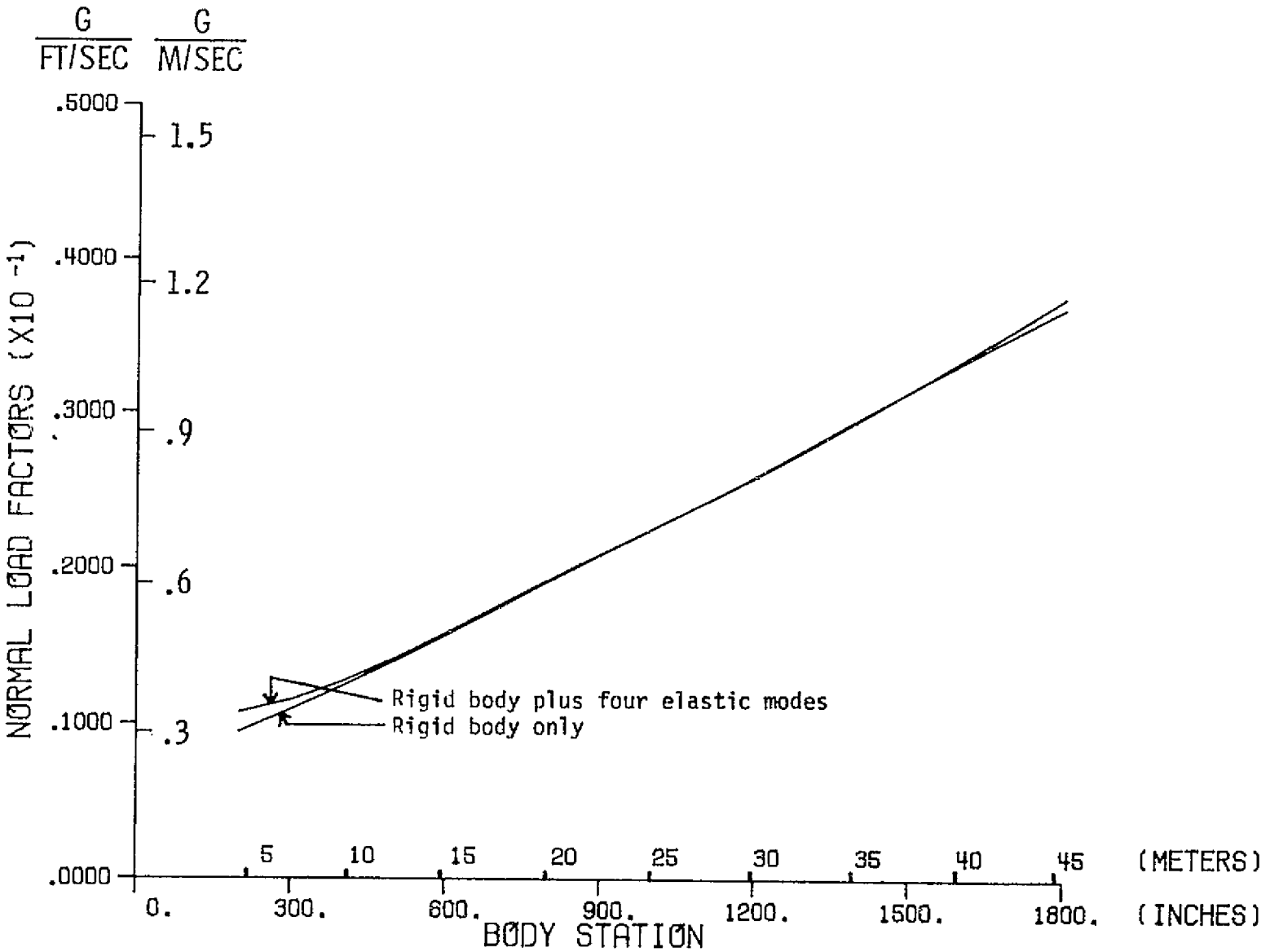

Figure 5.3 B-52H Unaugmented Vehicle. Mach .55, Altitude 610 m (2000 ft).

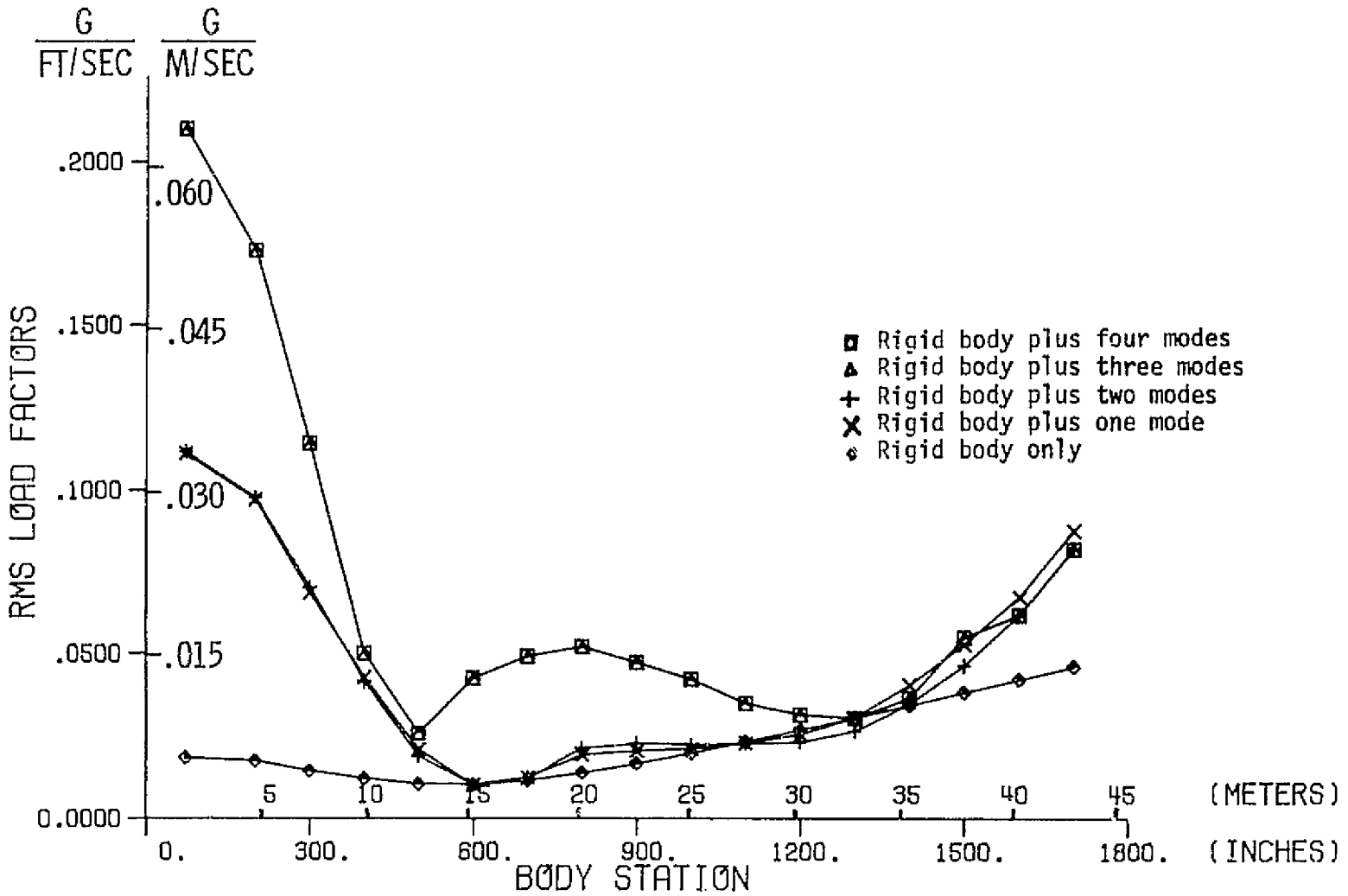

Figure 5.4 B-1 Unaugmented Vehicle Load Factors. Mach .85, Altitude 30 m (100 ft).

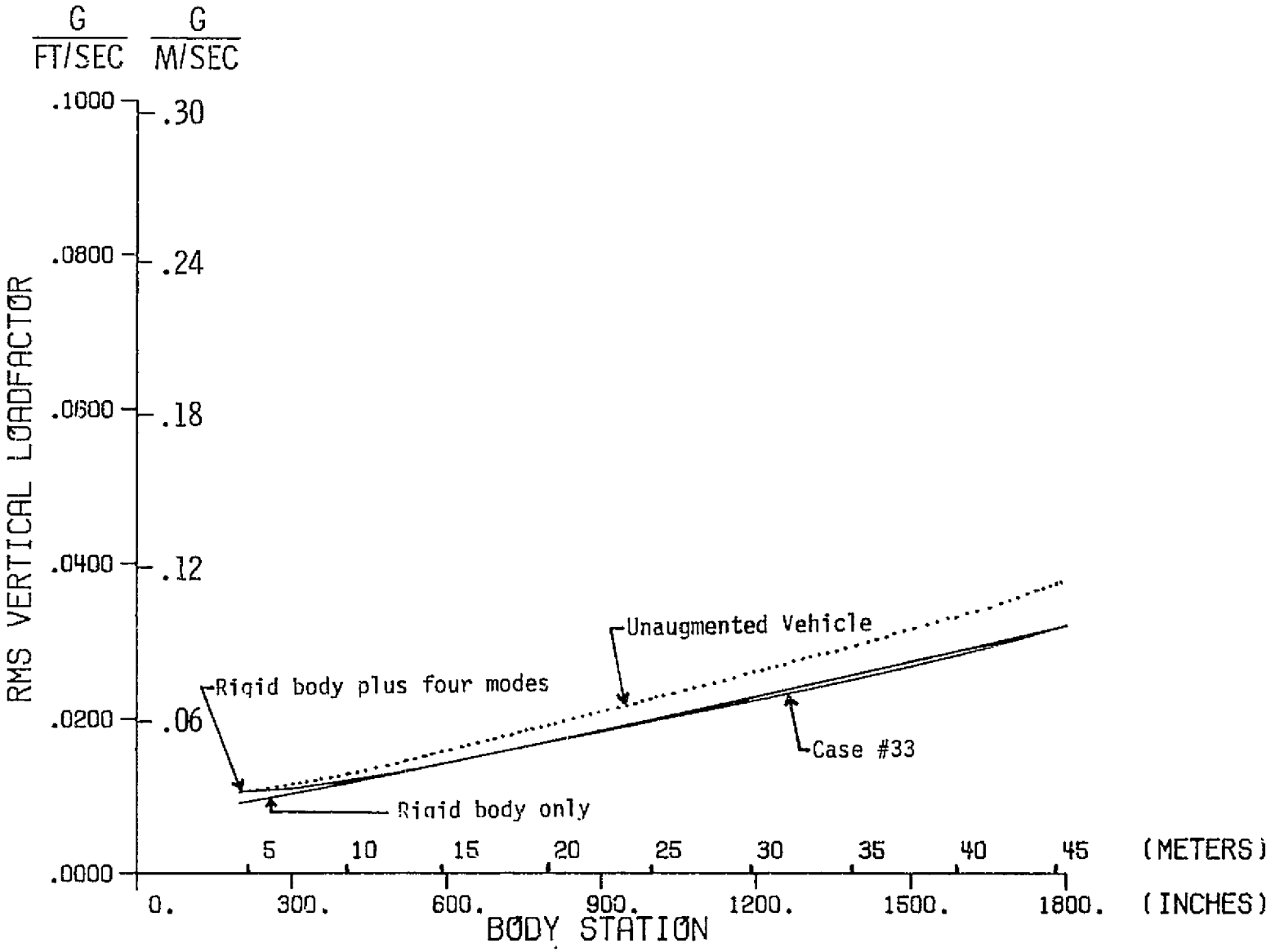

Figure 5.5 B-52H RSS, Restored Handling, Case #33. Mach .55, Altitude 610 m (2000 ft).

TABLE 5.3: RSS B-52H Ride With Restored Handling Qualities

B-52H CASE #	cg (Fuselage Station)	S_t	RSS EFFECT		SAS RESTORED VALUE		RQI
			$\omega_{n_{SP}}$	ζ_{SP}	$\omega_{n_{SP}}$	ζ_{SP}	
32	856.0	900	2.805	.5156	2.805	.5158	.9991
33	897.3	900	2.585	.4940	2.805	.5158	.8893
34	952.4	900	2.264	.4690	2.805	.5158	1.3222
35	952.4	600	.3208	Unstable	3.796	.7264	1.5183
36	897.3	600	.5403	Stable	3.005	.5840	1.3918
37+	856.0	600	1.153	.764	2.805	.5158	1.3553

apparently reduced. Figure 5.6 shows rigid body only plots from the unaugmented B-1 and from the RSS B-1 with handling restored. The rigid body line segment denoted by triangles for the RSS vehicle had consistently less curvature throughout the RSS B-1 data. Insufficient curvature and fidelity was generated on the B-52H rigid body load factor to generalize about this finding. In any case the apparent reduced coupling with the elastic modes generated a slightly better RSS B-1 ride (with restored handling characteristics) as shown by Table 5.4 with the RQI. Since the flight conditions were quite different no further generalizations about RSS should be made at this point. Research is needed into the coupling effects before generalizations about the elastic RSS can be attempted.

TABLE 5.4: RSS B-1 With Restored Handling Qualities

B-1 CASE #	cg (Fuselage Station)	S_t	RSS EFFECT		SAS RESTORED		RQI
			$\omega_{n_{SP}}$	ζ_{SP}	$\omega_{n_{SP}}$	ζ_{SP}	
27	1088.8	497.4	2.510	.464	2.793	.474	.9965
28	1125.6	497.4	2.070	.464	2.793	.474	.9714
29	1061.2	400	1.514	.663	2.793	.474	.9772
30	1061.2	450	2.263	.516	2.793	.474	.9966
31	1088.8	400	1.040	.839	2.793	.474	.9696
32+	1125.6	425	.857	.908	2.803	.475	.9664

+Load factor plots are shown in Appendix C, section C.5.

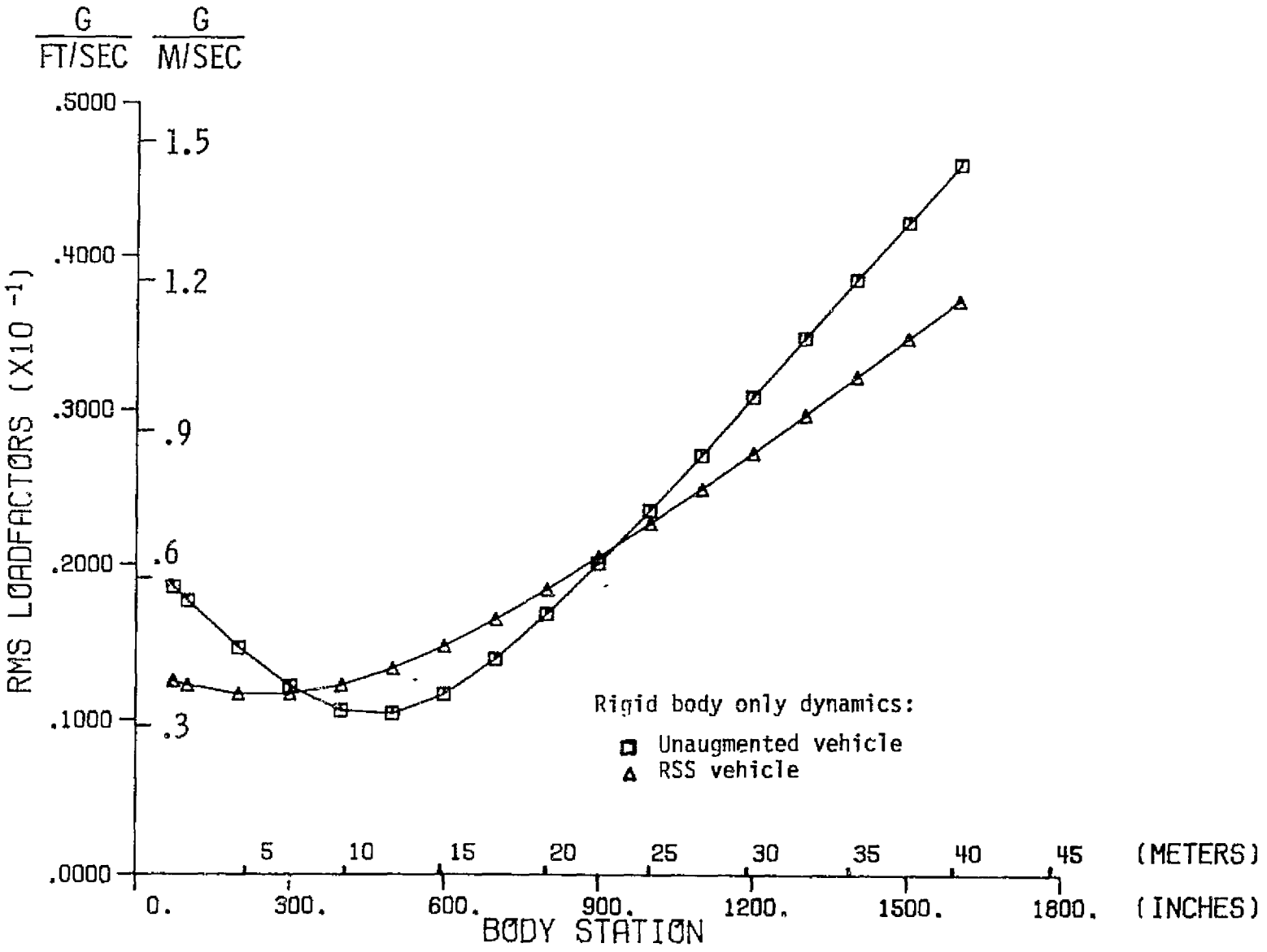

Figure 5.6 B-1 Rigid Body Load Factor Comparison.

In my opinion, the one generalization allowable concerning the B-1 is that RSS did not degrade the ride at this flight condition. At any other flight condition where the rigid body effects might contribute more to the load factor curve, the findings should be similar to the B-52H RSS. In addition inclusion of the SMCS (structural mode control system) on the B-1 will change the percentage contribution to overall ride by the rigid body.

5.7 Relaxed Static Stability Summary

RSS has a definite effect on RQ. This study has shown that the effect is not favorable when the original handling characteristics are restored on a more rigid aircraft. On the B-1 the restored handling resulted in a slightly better ride. This result may be modified when RSS is utilized in preliminary design or when appropriate elastic changes can be incorporated in RSS implementation on the B-1. A specific study should be made concerning the possible tradeoffs of increased RSS with restoration to different handling qualities. It would seem that some optimum RSS level exists as a design point for specific handling qualities.

The overwhelming percentage of total ride on the B-52H was due to the rigid body effects. Therefore, a larger effect was induced by RSS. By contrast, the B-1 had a relatively small RQ contribution (compared to the total) due to rigid body dynamics and was not as sensitive to the RSS effect. To completely verify the total B-1 effects the Swaim technique for estimating the coupling effects of the RSS implementation would be required as a minimum. This would insure that the decoupling effect mentioned above was not due to omission of changes to elastic mode aerodynamic terms due to RSS.

Chapter 6

RESULTS, CONCLUSIONS, AND RECOMMENDATIONS

6.1 Ride Quality Index Results and Recommendations

The utility of the RQI has been demonstrated in studying RQ under the influence of control law changes and variations of handling characteristics. The marketing appeal for a ride metric should be high since another decision index could now be placed at the consumer manager's disposal with minimum manufacturers' cost. Most companies do this kind of marketing now but there is no common denominator from which to judge the comparative ride quality that is being purchased.

Further study under the guidance of an aerospace industry marketing expert would clarify practical usage questions. For the USAF a study to find an avionics multiplier for specification values on the marketing index would give better guidance than now exists. A maximum operational avionics load factor value would provide an additional design point for the RQI.

6.2 B-52H and B-1 Ride Quality Conclusions and Recommendations

In summarizing the RQ investigations on the B-52H and B-1, I would like to re-emphasize the fact that no attempt was made to optimize the vehicle RQ. The technique demonstrated herein certainly would lend itself to a quadratic optimal performance or penalty function approach toward finding an optimal RQ feedback gain.

RQ is essentially independent of the control law type for equivalent closed loop dynamics. This finding was reasonable based on the current experience of control experts and was consistent on both of the test vehicles. Its import lies in the inference that the different numerator dynamics for two different control laws generate the same load factor output.

RQ is very sensitive to handling qualities criteria. Higher frequency and damping provide better RQ assuming no control, resonance, or flutter problems occur on a specific vehicle. This finding was consistent for both vehicles as well.

RSS by itself has a slightly favorable effect on RQ in that it decreases the slope of the rigid body RMS load factor curve. The overall effect is a decrease in the energy imparted to the aircraft aft of the cg. An increase occurs in the energy ahead of the cg. This finding was the same for both of the vehicles.

RSS with restored handling qualities degraded the RQ on the B-52H. This result was basically due to the higher RMS deflections on the elevator that were required to restore the handling characteristics desired. This effect was not evident with the B-1 flight condition evaluated in this study.

RSS slightly improved the B-1 overall RQ. Since RSS was treated as a rigid body phenomena no strong conclusion can be drawn from this finding. A preliminary interpretation would suggest that a favorable decoupling effect occurred in the highly elastic B-1 case, resulting in a better ride. An investigation of this interpretation is certainly justified. More importantly this investigation would be economical and straightforward with the elastic derivative synthesis process developed by Swaim and Fullman.

These conclusions raise other important questions which must be answered before a complete RQ criterion can be generated for large flexible vehicles of the future. A few of the important questions follow.

In the next ten to fifteen years retro-fit will be utilized by the airlines and USAF to update their airplanes. In order that RSS could be implemented as a fuel saving measure, several questions must be faced analytically as well as experimentally. First, is it possible to implement RSS by cargo or fuel management without appreciably changing the free-free elastic mode shape curves? This question is especially important on a highly flexible vehicle where the RQ is very sensitive to the mode shapes and the time history of the generalized coordinates.

Second, if the shapes do change, what is the maximum cg movement that could be implemented without degrading the ride?

From the preliminary design point of view, will RSS demonstrate the same load factor trends for new concept vehicles? This question involves the entire CCV concept and could affect major design decisions such as engine placement, configuration, and so on.

Another design question revolves around the favorable interaction of elastic modes for RQ. Is it possible to invoke maximum cancellation of significant elastic modes with the rigid body or other modes by utilizing a single control? Could this be done by artificially increasing the activity of a favorable mode?

Since the interaction phenomena exists, perhaps RSS with an active ride quality control system would generate more favorable cancellations. This might lead to significantly reduced load factor levels.

6.3 Summary

While this study ranged over a wide variety of handling characteristics and common control laws, it examined only two vehicles at two different flight conditions. Substantiating data is needed from other sources, vehicles, and flight conditions before conclusions and recommendations could be made for a general design logic. The ride quality metric should prove to be a valuable index for future parametric comparisons of this type.

REFERENCES

1. Bryson, A.E. and Ho, Yu-Chi, Applied Optimal Control, John Wiley & Sons, 1975.

2. Gelb, Arthur, et al, Applied Optimal Estimation, MIT Press, 1974.

3. Makers, D.T., "A Blended Feedback Variable for Control Augmentation Systems", AFFDL-TR-67-87, Wright-Patterson AFB, Ohio, 1967.

4. Perkins, W.R. and Cruz, J.B., Jr., Engineering of Dynamic Systems, Wiley & Sons, 1969.

5. Etkin, B., Dynamics of Atmospheric Flight, John Wiley & Sons, Inc., 1972.

6. McRuer, D., Ashkenas, I., and Graham, D., Aircraft Dynamics and Automatic Control, Princeton University Press, 1973.

7. Finck, R.D., Principal Investigator, Douglas Aircraft Division, USAF Stability and Control DATCOM, Air Force Flight Dynamics Laboratory, Wright-Patterson AFB, Ohio, 1960, revised 1975.

8. Heath, R.E., II, "State Variable Model of Wind Gusts", AFFDL/FGC-TM-72-12, Wright-Patterson AFB, Ohio, 1972.

9. Rustenburg, J.W., "Ride Quality Design Criteria for Aircraft With Active Mode Control Systems", ASD-TR-72-64, Wright-Patterson AFB, Ohio, 1972.

10. Rustenburg, J.W., "Development of Tracking Error Frequency Response Functions and Aircraft Ride Quality Design Criteria for Vertical and Lateral Vibration", ASD-TR-70-18, Wright-Patterson AFB, Ohio, 1971.

11. Jacobsen, I.D. and Rudrapatna, A.N., "Models of Subjective Response To In-Flight Motion Data", Technical Report 403209, Short-Haul Air Transportation Program, University of Virginia, 1973.

12. Swaim, R.L. and Fullman, D.G., "A Unique Formulation of Elastic Airplane Longitudinal Equations of Motion", to be published, Purdue University, West Lafayette, IN, 1976.

13. "B-52 CCV Control System Synthesis", by Boeing Company, Wichita Division, AFFDL-TR-74-92, Volume II, Wright-Patterson AFB, Ohio, 1975.

14. "Critical Analysis of B-52 Stability Augmentation and Flight Control Systems For Improved Structural Life", Parts I-V, D3-6434-1 thru -5, Boeing Company, Wichita, KA, 1965.

15. Wykes, J.H., "B-1 Flexible Vehicle Equations of Motion For Ride Quality, Terrain Following, and Handling Qualities Studies", Internal Document TFD-71-430-1, North American Rockwell, Los Angeles, CA, 1971, revised 1973.

16. Chalk, C.R., et al., "Background Information and User Guide for MIL-F-8785B(ASG), 'Military Specification - Flying Qualities of Piloted Airplanes'," AFFDL-TR-69-72, Air Force Flight Dynamics Laboratory, Wright-Patterson AFB, Ohio, 1969.

Appendix A

LONGITUDINAL EQUATIONS OF MOTION

A.1 General Description and Assumptions.

The vector differential equations A.1 and A.2 provide the origin of the mathematical model for elastic vehicles.

$$\frac{dp}{dt} = F \tag{A.1}$$

$$\frac{dH}{dt} = M \tag{A.2}$$

where p Linear momentum vector

H Angular momentum vector

F Resultant sum of all externally applied forces

M Sum of all applied torques.

With the assumptions that:

1) the earth is an inertial reference in space

2) the airframe is initially a rigid structure

3) mass and mass distributions of the vehicle are constant

4) the vertical or XZ plane is a plane of symmetry

5) perturbations from the cruise conditions allow small angle assumptions

6) quasi-steady flow is sufficient to describe the aerodynamic perturbations

7) the vehicle is at cruise-level conditions

8) the flight path is over a flat surface earth

The Laplace transformed longitudinal equations of motion are given in A.3:

$$\begin{bmatrix} s-X_u & -\dot{X}_w s-X_w & -X_q s+g\cos\gamma_0 \\ -Z_u & s-\dot{Z}_w s-Z_w & -Us-Z_q s+g\sin\gamma_0 \\ -M_u & -\dot{M}_w s-M_w & s^2-sM_q \end{bmatrix} \begin{bmatrix} u \\ w \\ \theta \end{bmatrix} = \begin{bmatrix} X_{\delta_e} & X_u & \dot{X}_w s+X_w \\ Z_{\delta_e} & Z_u & \dot{Z}_w s+Z_w-\frac{Z_q s}{U} \\ M_{\delta_e} & M_u & \dot{M}_w s+M_w-\frac{M_q s}{U} \end{bmatrix} \begin{bmatrix} \delta_e \\ u_g \\ w_g \end{bmatrix} \quad (A.3)$$

The stability axis sign convention is depicted in Figure A.1. Note that the vertical gust velocity is defined positive in the negative Z axis direction thereby inducing a positive angle of attack.

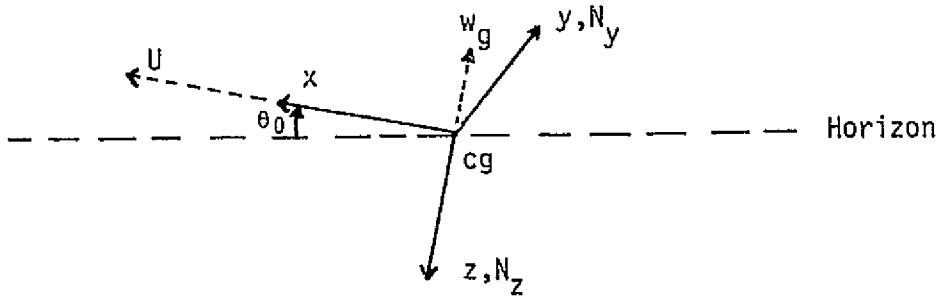

Figure A.1 Vehicle Stability Axis Sign Convention.

For our purposes the perturbation of forward velocity has an extremely small effect on vertical load factors. Hence, the first equation is dropped and the short period, rigid body equations of motion remain. To these equations we add the equations of motion corresponding to the generalized coordinates of the four lowest frequency elastic modes of each vehicle. The instantaneous generalized coordinate value of a particular mode multiplied by the mode shape yields the instantaneous displacement of the mode at that point. Utilizing this orthogonal

$$\begin{bmatrix} (s-Z_w) & -Us & -Z_{\xi_1} & -Z_{\xi_2} & -Z_{\xi_3} & -Z_{\xi_4} \\ -M_{\dot{w}}s-M_w & (s^2-M_q s) & -M_{\xi_1} & -M_{\xi_2} & -M_{\xi_3} & -M_{\xi_4} \\ -F_{1_w} & 0 & (s^2+2\zeta_1\omega_1 s+\omega_1^2) & -F_{1_{\xi_2}} & -F_{1_{\xi_3}} & -F_{1_{\xi_4}} \\ -F_{2_w} & 0 & -F_{2_{\xi_1}} & (s^2+2\zeta_2\omega_2 s+\omega_2^2) & -F_{2_{\xi_3}} & -F_{2_{\xi_4}} \\ -F_{3_w} & 0 & -F_{3_{\xi_1}} & -F_{3_{\xi_2}} & (s^2+2\zeta_3\omega_3 s+\omega_3^2) & -F_{3_{\xi_4}} \\ -F_{4_w} & 0 & -F_{4_{\xi_1}} & -F_{4_{\xi_2}} & -F_{4_{\xi_3}} & (s^2+2\zeta_4\omega_4 s+\omega_4^2) \end{bmatrix} \begin{bmatrix} w(s) \\ \theta(s) \\ \xi_1(s) \\ \xi_2(s) \\ \xi_3(s) \\ \xi_4(s) \end{bmatrix} =$$

$$\begin{bmatrix} Z_{\delta_e} \\ M_{\delta_e} \\ F_{1_{\delta_e}} \\ F_{2_\delta} \\ F_{3_{\delta_e}} \\ F_{4_{\delta_e}} \end{bmatrix} \delta_e(s) + \begin{bmatrix} Z_w & 0 \\ M_w & M_q \\ F_{1_w} & 0 \\ F_{2_w} & 0 \\ F_{3_w} & 0 \\ F_{4_w} & 0 \end{bmatrix} \begin{bmatrix} w_g(s) \\ q_g(s) \end{bmatrix} \qquad (A.4)$$

where F_{i_j} represents the generalized force change of the ith mode due to a change in the state j.

mode model, which is most common in aeroelasticity, and equation A.3, we can write the elastic vehicle equations as shown in equation A.4. Rewriting the system as a 10th order set of first order linear differential equations, equation A.4 becomes the familiar control equation A.5. The approximation $w = U\alpha$ is used to transform the vertical velocity to the perturbation angle of attack. Note that the states in A.5 are arranged in a slightly different manner compared to the Laplace domain system.

$$\dot{x}^* = A^*x^* + B^*u + M^*x_g^* \tag{A.5}$$

where $x^{*'} = \lfloor \xi_1 \ \xi_2 \ \xi_3 \ \xi_4 \ \alpha \ \dot{\theta} \ \dot{\xi}_1 \ \dot{\xi}_2 \ \dot{\xi}_3 \ \dot{\xi}_4 \rfloor$

$x_g^{*'} = \lfloor \alpha_g \ q_g \rfloor$

A.2 Turbulence Model

The Dryden power spectral density representation of turbulence is modeled as a set of three first order linear differential equations. This model is due to Heath and is derived in reference 8.

The temporal frequency representations of the angle of attack and pitch gust power spectra are:

$$\Phi_{\alpha_g}(\omega) = \sigma_{w_g}^2 \frac{L_w}{\pi U^3} \frac{1 + 3\left(\frac{L_w \omega}{U}\right)^2}{\left[1 + \left(\frac{L_w \omega}{U}\right)^2\right]^2}$$

$$\Phi_{q_g}(\omega) = \Phi_{\alpha_g}(\omega) \frac{\omega^2}{1 + \left(\frac{4b\omega}{\pi U}\right)^2}$$

where σ_{w_g} RMS vertical gust intensity (.30 m/sec (1 ft/sec) throughout this investigation)

L_w Gust scale which depends on the altitude

U Average velocity of the vehicle

b Wing span

Table A.1 shows the appropriate values for these factors at the flight conditions used in this study.

TABLE A.1: Gust Specifications For The Study Vehicles

B-52H Value	Factor	B-1 Value
.30 m/sec (1 ft/sec)	σ_{W_g}	.30 m/sec (1 ft/sec)
533 m (1750 ft)	L_W	30 m (100 ft)
186 m/sec (608.8 ft/sec)	U	289 m/sec (949.45 ft/sec)
56 m (185 ft)	b	42 m (136.68 ft)

Modeling the gusts above as a white noise input to a linear system, the spectra can be represented as a system of linear, first order differential equations shown in equation A.6:

$$\begin{bmatrix} \dot{\alpha}_{g_1} \\ \dot{\alpha}_g \\ \dot{q}_g \end{bmatrix} = [A_g] \begin{bmatrix} \alpha_{g_1} \\ \alpha_g \\ q_g \end{bmatrix} + G^* \eta \qquad (A.6)$$

where η is scalar unit white noise in the time domain
Using A.6 as the forcing system we can now rewrite A.5 with A.6 appended as follows:

$$\begin{bmatrix} \dot{x}^* \\ \dot{x}_g \end{bmatrix} = \begin{bmatrix} A^* & M^* \\ 0 & A_g \end{bmatrix} \begin{bmatrix} x^* \\ x_g \end{bmatrix} + \begin{bmatrix} B^* \\ 0 \end{bmatrix} u + \begin{bmatrix} 0 \\ G^* \end{bmatrix} \eta \qquad (A.7)$$

Simplifying this simultaneous set into single matrix elements, the general equations of motion for both vehicles are written in the form A.8:

$$\dot{x} = Ax + Bu + G\eta \qquad (A.8)$$

$$\text{where } x' = \left| \xi_1 \ \xi_2 \ \xi_3 \ \xi_4 \ \alpha \ \dot{\theta} \ \dot{\xi}_1 \ \dot{\xi}_2 \ \dot{\xi}_3 \ \dot{\xi}_4 \ \alpha_{g_1}, \ \alpha_g, \ q_g \right| \qquad (A.9)$$

A.3 B-52H Equations of Motion

The B-52H equations were derived from the 18 degree of freedom time domain equations in reference 14. The four lowest frequency elastic modes were used in this study. The eigenvalues are shown in Table A.2. The [A*M*], B*, and G* matrices derived from the documents supplied by Boeing Company are given by Tables A.3, A.4, and A.5 respectively. Table A.6 specifies the A_g gust coefficient matrix which is appended to the vehicle state equations in equation A.7. The mode shapes, associated locations, and distance to the cg (in feet) are given in Table A.7.

TABLE A.2: B-52H Bare Airframe Coupled Eigenvalues

Mode	Roots	Frequency	Damping
Short Period	-1.447 ± 2.404i	2.8066	.5157
1	.919 ± 5.679i	5.7531	.1598
2	.959 ± 11.513i	11.5530	.0830
3	.140 ± 12.470i	12.4710	.0112
4	.820 ± 14.804i	14.8270	.0553

TABLE A.4: B-52H Control Matrix B* (10x1)

0	0	0	0
-5.52E - 02	-3.99E + 00	3.36E + 01	-1.28E + 00
9.12E + 00	-2.92E + 01		

TABLE A.5: B-52H White Noise Matrix, G* (3x1)

1.00000	1.67804E - 03	4.33710E - 03

TABLE A.6 B-52H Gust Matrix, A_g (3x3)

-3.4789E - 01	0	0
-2.4648E - 04	-3.4789E - 01	0
-6.3775E - 04	-8.9916E - 01	-2.5846E + 00

TABLE A.3: B-52H [A* : M*] Matrix (10x13)

η_1	η_2	η_3	η_4	α	$\dot{\theta}$	$\dot{\eta}_1$
$\dot{\eta}_2$	$\dot{\eta}_3$	$\dot{\eta}_4$	α_{g_1}	α_g	q_g	
0	0	0	0	0	0	1.000D+00
0	0	0	0	0	0	
0	0	0	0	0	0	0
1.000D+00	0	0	0	0	0	
0	0	0	0	0	0	0
0	1.000D+00	0	0	0	0	
0	0	0	0	0	0	0
0	0	1.000D+00	0	0	0	
-4.210D-03	-2.692D-01	-8.073D-02	1.406D-01	-1.352D+00	9.498D-01	-6.041D-04
-9.058D-03	-2.360D-03	4.076D-03	0	-1.352D+00	0	
-3.817D-02	-4.688D+00	8.305D-01	-6.056D-01	-7.556D+00	-1.738D+00	6.295D-03
-1.722D-01	5.847D-02	-6.321D-02	0	-7.556D+00	-1.738D+00	
-3.368D+01	-1.277D+02	-1.843D+01	4.293D+01	-1.014D+02	-1.078D-01	-2.217D+00
-4.241D+00	-7.373D-01	1.098D+00	0	-1.014D+02	0	
-6.873D-01	-1.326D+02	-9.719D-01	4.247D+00	-3.629D+01	-2.425D+00	-2.442D-01
-1.290D+00	8.058D-02	-9.337D-04	0	-3.629D+01	0	
-8.021D-01	2.026D+00	-1.548D+02	3.074D+00	7.820D+00	1.447D+00	-8.578D-02
1.511D-01	-3.719D-01	4.690D-01	0	7.820D+00	0	
2.642D-01	-3.110D+01	7.123D+00	-2.222D+02	-3.837D+01	-4.818D+00	-7.347D-02
-9.265D-01	1.243D+00	-1.604D+00	0	-3.837D+01	0	

Table A.7: B-52H Mode Shapes

Fuselage Station	Distance From cg	Mode 1	Mode 2	Mode 3	Mode 4
200.000000	54.666667	0	.375000	-.252000	.340000
300.000000	46.333333	-.020000	.322000	-.195000	.240000
400.000000	38.000000	-.039000	.277000	-.143000	.155000
500.000000	29.666667	-.060000	.237000	-.100000	.081000
600.000000	21.333333	-.080000	.208000	-.063000	.025000
700.000000	13.000000	-.100000	.183000	-.032000	-.023000
800.000000	4.666667	-.124000	.162000	-.013000	-.055000
900.000000	-3.666667	-.147000	.142000	-.003000	-.072000
1000.000000	-12.000000	-.175000	.127000	-.005000	-.079000
1100.000000	-20.333333	-.203000	.112000	-.016000	-.070000
1200.000000	-28.666667	-.234000	.104000	-.040000	-.045000
1300.000000	-37.000000	-.265000	.100000	-.072000	-.008000
1400.000000	-45.333333	-.300000	.095000	-.115000	.045000
1500.000000	-53.666667	-.338000	.090000	-.165000	.116000
1600.000000	-62.000000	-.375000	.087000	-.230000	.205000
1700.000000	-70.333333	-.415000	.086000	-.300000	.305000
1800.000000	-78.666667	-.455000	.089000	-.380000	.420000

A.4 B-1 Equations of Motion

The low level penetration flight condition for the B-1 was supplied by the B-1 System Program Office at Wright-Patterson AFB from Rockwell International documents. The values used in these equations of motion were based on preliminary aerodynamic analyses, but are closely representative of the vehicle now flying. The time domain format for the longitudinal equations shown below was decoupled from the complete vehicle set given in reference 15 The eigenvalues for the longitudinal set are shown in Table A.8.

TABLE A.8: B-1 Bare Airframe Coupled Eigenvalues

Mode	Roots	Frequency	Damping
Short Period	-1.3136 ± 2.4617i	2.790	.4708
1	- .6335 ± 13.2574i	13.272	.0477
2	- .4715 ± 21.3522i	21.357	.0221
3	- .2038 ± 22.0188i	22.020	.0093
4	-4.4861 ± 22.0144i	22.467	.1997

The values for the unaugmented vehicle equations are given by the [A*M*], B*, and G* matrices in Tables A.9, A.10, and A.11 respectively. No structural mode control system dynamics were included in this study. Table A.12 gives the B-1 flight condition values for the gust coefficients A_g. Table A.13 shows the mode shape information for the B-1.

TABLE A.10: B-1 Control Matrix, B* (10x1)

0	0	0	0
-2.8840E - 01	-1.5025E + 01	-2.2303E + 01	-2.1523E + 02
6.1356E + 02	1.0785E - 01		

TABLE A.11: B-1 White Noise Matrix, G* (3x1)

1.0000E + 00	5.6210E - 03	3.0669E - 02

TABLE A.9: B-1 [A* : M*] Matrix (10x13)

η_1	η_2	η_3	η_4	α	$\dot{\theta}$	$\dot{\eta}_1$
$\dot{\eta}_2$	$\dot{\eta}_3$	$\dot{\eta}_4$	α_{g_1}	α_g	q_g	
0	0	0	0	0	0	1.000D+00
0	0	0	0	0	0	
0	0	0	0	0	0	0
1.000D+00	0	0	0	0	0	
0	0	0	0	0	0	0
0	1.000D+00	0	0	0	0	
0	0	0	0	0	0	0
0	0	1.000D+00	0	0	0	
-8.940D-03	9.525D-02	4.618D-03	-4.346D-03	-1.208D+00	9.440D-01	-2.130D-04
2.590D-03	1.526D-04	-4.998D-06	0	-1.204D+00	5.472D-02	
-1.842D-01	-1.248D-01	2.072D-01	-9.171D-02	-7.059D+00	-2.018D+00	-7.438D-03
4.972D-02	6.963D-03	-2.004D-03	0	-7.049D+00	-1.915D+00	
-1.774D+02	-1.568D+01	6.190D+01	2.088D+01	-7.383D+02	-1.333D+02	-1.139D+00
-2.770D-01	9.159D-01	-1.977D-01	0	-7.371D+02	-1.679D+02	
1.407D+01	-5.061D+02	6.593D+00	1.124D+01	1.300D+03	1.633D+01	2.351D-01
-8.596D+00	1.131D-01	1.120D-01	0	1.298D+03	2.902D+01	
6.990D+00	3.458D+01	-4.565D+02	3.457D+00	7.577D+02	5.595D+01	-1.219D-01
3.784D+00	-8.485D-01	-2.535D-01	0	7.564D+02	6.180D+01	
1.623D-02	-9.700D-02	7.112D-03	-4.849D+02	1.688D+00	3.990D-02	-3.292D-04
2.427D-03	-2.764D-04	-4.088D-01	0	1.697D+00	3.817D-02	

TABLE A.12: B-1 Gust Matrix, A_g (3x3)

-9.495E + 00	0	0
-2.256E - 02	-9.495E + 00	0
-1.231E - 01		-5.456E + 00

Table A.13: B-1 Mode Shapes

Fuselage Station	Distance From cg	Mode 1	Mode 2	Mode 3	Mode 4
72.000000	82.433333	1.000000	1.000000	1.000000	1.000000
100.000000	80.100000	.880000	.900000	.805000	.880000
200.000000	71.766667	.625000	.750000	.500000	.505000
300.000000	63.433333	.394000	.400000	.180000	.140000
400.000000	55.100000	.187000	.200000	-.075000	-.100000
500.000000	46.766667	.014000	0	-.202000	-.205000
600.000000	38.433333	-.038000	0	-.240000	-.280000
700.000000	30.100000	-.130000	-.100000	-.240000	-.280000
800.000000	21.766667	-.135000	-.100000	-.205000	-.225000
900.000000	13.433333	-.120000	-.050000	-.175000	-.200000
1000.000000	5.100000	-.105000	0	-.125000	-.160000
1100.000000	-3.233333	-.070000	.100000	-.100000	-.125000
1200.000000	-11.566667	0	.200000	-.061000	-.090000
1300.000000	-19.900000	.100000	.360000	-.041000	-.030000
1400.000000	-28.233333	.205000	.460000	-.121000	.040000
1500.000000	-36.566667	.322000	.780000	.005000	.150000
1600.000000	-44.900000	.490000	1.000000	.020000	.225000

Appendix B

CASE DOCUMENTATIONS

B.1 Discussion

The tables B.1 and B.3 are complete outlines of the control law and handling quality parameterizations which were run on the B-52H and B-1 vertical load factor cases. The full state gain matrices are identified by case # in Table B.2 and B.4.

TABLE B.1: B-52H Case Control List

Case #	Type SAS	ζ_{SP}	$\omega_{n_{SP}}$	u = -Kx Gain 1	Gain 2
1	$\dot{\theta}$	.5157	2.806		0.
2	$\dot{\theta}$	.404	2.635		-.2
3	$\dot{\theta}$	.617	2.970		+.2
4	$\dot{\theta}$	.712	3.126		+.4
5	C*	.3403	2.521	-.0005	0.
6	C*	.514	2.779	-.0005	+.3
7	C*	.482	2.751	-.0001	.0
8	C*	.506	2.806	+.0003	-.2
9	C*	.856	3.402	+.0004	+.5
10	$\theta/\dot{\theta}$	.359	2.754	.25	-.2
11	$\theta/\dot{\theta}$	.723	3.272	.25	.5
12	$\theta/\dot{\theta}$	.706	3.497	.75	.6
13	$\theta/\dot{\theta}$	.528	2.982	.25	.1
14	$\theta/\dot{\theta}$	.297	2.677	.25	-.3
15	Full State	.5157	2.806		
16	Full State	.325	2.806		
17	Full State	.8176	2.806		
18	Full State	.5157	2.806		

TABLE B.1, cont.

19	Full State	.325	2.806
20	Full State	.8176	2.806
21	Full State		$\dot{\theta}$ Comparison
22	Full State	.5157	3.000
23	Full State	.5157	3.400
24	Full State	.5157	2.806
25	Full State	.325	2.806
26	Full State	.8176	2.806
27*	Full State	.5157	2.806
28*	Full State	.325	2.806
29*	Full State	.8176	2.806
30	Full State	.8176	3.000
31	Full State	.8175	3.400
32	RSS Test Case	.5158	2.805
33	RSS Restored HQ	.5158	2.805
34	RSS Restored HQ	.5158	2.805
35	RSS Restored HQ	.7264	3.796
36	RSS Restored HQ	.5840	3.005
37	RSS Restored HQ	.5158	2.805
38	RSS No Restoration	.5158	2.805
39	RSS Rigid Only	.5470	2.640
40	RSS Rigid Only	.5920	2.410
41	RSS Rigid Only	.6550	2.160
42	RSS Rigid Only	.7480	1.860
43	RSS Rigid Only	.5770	2.350
44	RSS Rigid Only	.6290	2.010
45	RSS Rigid Only	.7380	1.700
46	RSS Rigid Only	1.000	2.207

*Increased damping on elastic modes

TABLE B.2: B-52H Full State Control Gains

Case #	K_1	K_2	K_3	K_4	K_5	K_6	K_7	K_8	K_9	K_{10}
24	0	0	0	0	0	0	0	0	0	0
25	-.004	.06	-.01	.02	-.34	.28	-.0006	-.007	.002	-.001
26	.006	-.09	.03	-.03	.54	-.44	.001	.01	-.002	.001
27	-.005	.59	-1.40	- 01	.19	-.02	.001	-.08	.329	-.024
28	-.01	.73	-1.73	-.85	-.14	.25	.009	-.08	.313	-.03
29	.004	.38	-.85	-1.00	.71	-.45	.003	-.08	.35	-.02
30	.008	-.11	.03	-.03	.34	-.52	.001	.015	-.003	.002
31	.01	-.13	.04	-.04	-.14	-.68	.001	.022	-.003	.002
					RSS RESTORED HQ					
32	0	0	0	0	0	0	0	0	0	0
33	.004	-.004	.004	-.005	-.39	-.15	.0001	.005	-.0007	.0004
34	-.06	.58	-.17	.18	3.84	3.69	-.002	-.14	.02	-.01
35	-.14	2.10	.302	.43	14.05	6.1	-.03	-.36	.01	-.03
36	.02	.15	.11	-.002	-3.95	-1.15	-.007	.04	-.007	.0004
37	.008	.02	.003	-.003	-1.57	-.321	-.0005	.01	-.001	.0004

TABLE B.3: B-1 Case Control List

Case #	Type SAS	ζ_{SP}	$\omega_{n_{SP}}$	$u = -Kx$ Gain 1	Gain 2
1	$\dot{\theta}$	.4708	2.790		0.
2	$\dot{\theta}$	.6551	2.981		+.1
3	$\dot{\theta}$	.8240	3.168		+.2
4	$\dot{\theta}$	.2650	2.594		-.1
5	C*	.3220	2.483	-.0005	+.4
6	C*	.3100	2.504	-.0004	+.3
7	C*	.5230	2.685	-.0004	+.4
8	C*	.7160	2.862	-.0004	+.5
9	C*	.6410	3.013	+.0001	0.
10	C*	.8080	3.204	+.0001	+.1
11	C*	.4340	2.881	+.0003	-.3
12	C*	.6120	3.084	+.0003	-.2
13	C*	.5840	3.160	+.0005	-.4
14	C*	.8890	3.570	+.0005	-.2
15	$\theta/\dot{\theta}$	.4230	2.955	+.1	0.
16	$\theta/\dot{\theta}$	.7760	3.288	+.1	+.2
17	$\theta/\dot{\theta}$	.6950	3.550	+.3	+.2
18	$\theta/\dot{\theta}$	.8170	3.817	+.4	+.3
19	Full State	.4716	2.790		
20	Full State	.4707	2.790		
21	Full State	.4707	2.790	Increased damping ζ_1, ζ_3	
22	Full State	.4707	2.790	Increased damping ζ_1, ζ_3	
23	Full State	.6551	2.790		
24	Full State	.6132	2.980		
25	Full State	1.0000	0.229		
26	Full State	.2850	2.594		
27	RSS Restored HQ	.4740	2.793		
28	RSS Restored HQ	.4740	2.793		
29	RSS Restored HQ	.4740	2.793		
30	RSS Restored HQ	.4740	2.793		

TABLE B.3, cont.

31	RSS Restored HQ	.4740	2.793	
32	RSS Restored HQ	.4750	2.803	
33	Full State	.4708	2.790	No q_g effect
34	Full State	.8240	3.168	
35	Full State	.4708	2.790	

TABLE B.4: B-1 Full State Control Gains

Case #	K_1	K_2	K_3	K_4	K_5	K_6	K_7	K_8	K_9	K_{10}
19	0	0	0	0	0	0	0	0	0	0
20	0	0	0	0	0	0	0	0	0	0
21	-.01	-.16	-.19	659.	-1.04	-.17	-.002	.02	-.003	28.97
22	-.02	-.06	-.24	894.6	-1.92	-.21	-.003	.03	-.002	27.43
23	-.0008	.003	.001	-1.73	.06	-.08	-.00003	.0001	-.00007	.23
24	-.0007	.003	.001	-1.72	-.02	-.08	-.00002	.0001	-.00007	.22
25	-.002	.008	.001	-.01	.66	-.16	.0001	.0002	-.000036	.000096
26	-.007	-.26	-.19	566.9	-.50	-.076	-.002	.0186	-.004	33.66
					RSS HQ RESTORED					
27	-.0001	.002	.0001	.0001	-.11	-.03	.00003	-.00001	-.00008	.000004
28	-.0002	.004	.003	.001	-.28	-.06	.00008	-.00005	-.00002	.00001
29	-.00002	.004	.0001	-.001	-.43	-.05	.00007	-.0001	-.00002	.00001
30	-.00002	.002	.00007	-.0002	-.21	-.02	.00004	-.00005	-.000008	.000006
31	-.00008	.005	.0002	-.003	-.54	-.72	.0001	-.0001	-.00003	.00001
32	-.0002	.007	.0004	.0005	-.61	-.09	.0001	-.0002	-.00004	.00002

Appendix C

NUMERICAL ANALYSES

C.1 Computational Algorithms

Figure C.1 shows the logic and names of the subroutines which accomplished all of the computing for these studies. Various versions of these routines are available in the Purdue University School of Aeronautics and Astronautics Guidance and Control Laboratory. The generalized program RIDEQ can be used to do all general load factor tasks and is referenced here in terms of subroutine names. RIDEQ was developed as an all purpose program by Mr. Dan Raymer. The subroutines in RIDEQ were due to Mr. Andrew Hinsdale. A user guide is available in the Guidance and Control Laboratory for RIDEQ.

C.2 Subroutine TRANSIT

This algorithm for computation of the linear covariance equation solution deserves special mention. The technique from reference 2 is programmed in variable dimensions and requires only 20-30 seconds on the Purdue CDC-6500. It uses a step size of 0.08 → .1 very efficiently. Iterative checking on the solution accuracy allows early completion if the spectral radii of the matrices are appropriately small.

The physical requirement for a stable final vehicle configuration manifests itself in the requirement that the spectral radius of the A matrix in C.1 be less than unity.

$$A\,E\{xx'\} + E\{xx'\}\,A' + GG' = 0 \qquad (C.1)$$

To review the computational procedure, let $E\{xx'\} \triangleq P$ and

$$\dot{P} = AP + PA' + GG' \qquad (C.2)$$

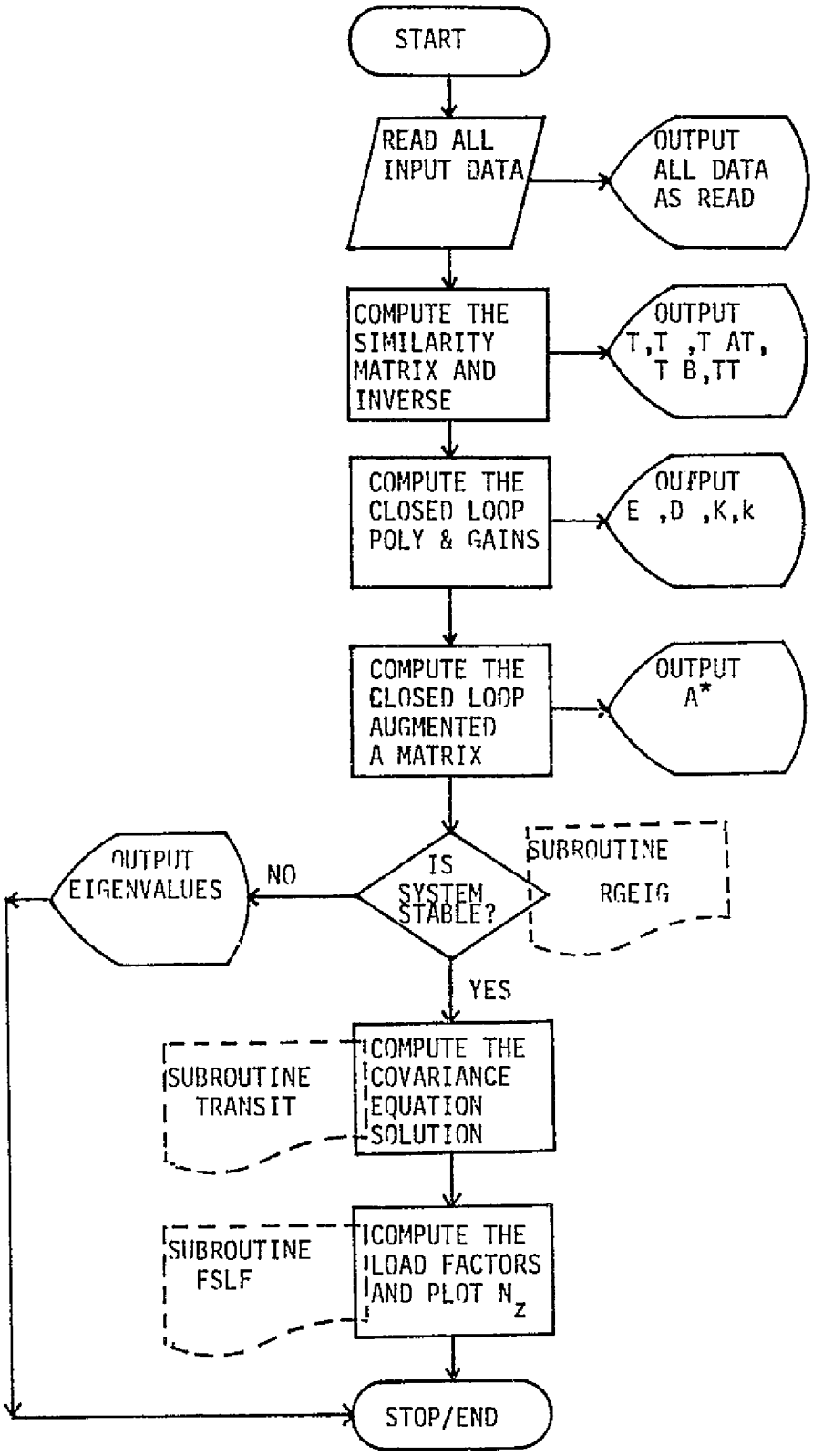

Figure C.1 RIDEQ Load Factors Algorithm.

Define

$$M = \begin{bmatrix} -A' & \vdots & 0 \\ \cdots\cdots & \vdots & \cdots \\ GG' & \vdots & A \end{bmatrix} \tag{C.3}$$

The state transition matrix for C.1 can be represented by:

$$e^{M\tau} = I + M\tau + \frac{I}{2!} M^2\tau^2 + \ldots \tag{C.4}$$

Then let:

$$e^{M\tau} = \begin{bmatrix} M_1 & \vdots & 0 \\ \cdots\cdots & \vdots & \cdots \\ M_2 & \vdots & M_3 \end{bmatrix} \tag{C.5}$$

Let $\tau = t_2 - t_1 = \Delta t$ and t_2 is the next point in time where P is evaluated

$$P(t_2) = M_2 M_3' + M_3 P(t_1) M_3' \tag{C.6}$$

After a certain number of iterations we minimize off diagonal round-off error by:

$$P(t_i) = [P(t_i) + P'(t_i)][\tfrac{1}{2}] \tag{C.7}$$

Substitution into C.2 to test $\dot{P} \to 0$ and prescription of a stopping precision are the remaining steps for this algorithm.

C.3 Phase Variable Canonical Matrix Calculations

The solution of C.1 is sensitive to matrix ill-conditioning in the sense that the matrix A should be reasonably well distributed by element magnitudes. We found that the form C.8 would lead to two or three orders of magnitude error in the final covariance solution matrix.

$$A = \begin{bmatrix} 0 & 1 & 0 & \cdots & 0 \\ 0 & 0 & 1 & \ddots & 0 \\ 0 & & \ddots & \ddots & \vdots \\ \vdots & & & \ddots & 0 \\ 0 & \cdots & \cdots & 0 & 1 \\ -d_0 & -d_1 & -d_2 & \cdots & -d_{n-1} \end{bmatrix} \qquad (C.8)$$

A double precision routine was written to test TRANSIT under these same conditions. The test case showed little improvement and would have required almost five times more CPU time to complete the computations for the covariance matrix. As a result all TRANSIT computations were done in the physical state variable form. That is, the A matrix was not used in TRANSIT in the phase variable canonical form.

C.4 Transformation Matrix T

Another form of the same matrix ill-conditioning appeared in the solution check on the similarity transform, T. After forming the T matrix we formed and printed the $[T^{-1}AT]$ combination which should have been the phase variable canonical form mentioned above.

All rows and columns of the check case were very accurate except the first three or four columns. These columns showed great sensitivity to the accuracy with which the T matrix was originally formed. This was especially true with respect to the coefficients of the open loop characteristic equation.

It was found that a sufficiently accurate check could be attained if the transformation matrix routine was supplied with 16 digit (single precision) data but was computed in double precision modes. Of course the accuracy of the study vehicle data was not known to this extent. Hence, the extension of the subroutine hand-off accuracy was a theoretical exercise in computation and had no bearing on the outcome or results of the studies.

C.5 Load Factor Plots for Significant Cases

This section contains the plots for significant cases in the required comparisons of the main body of this work. The case number is specified in each of the figure captions.

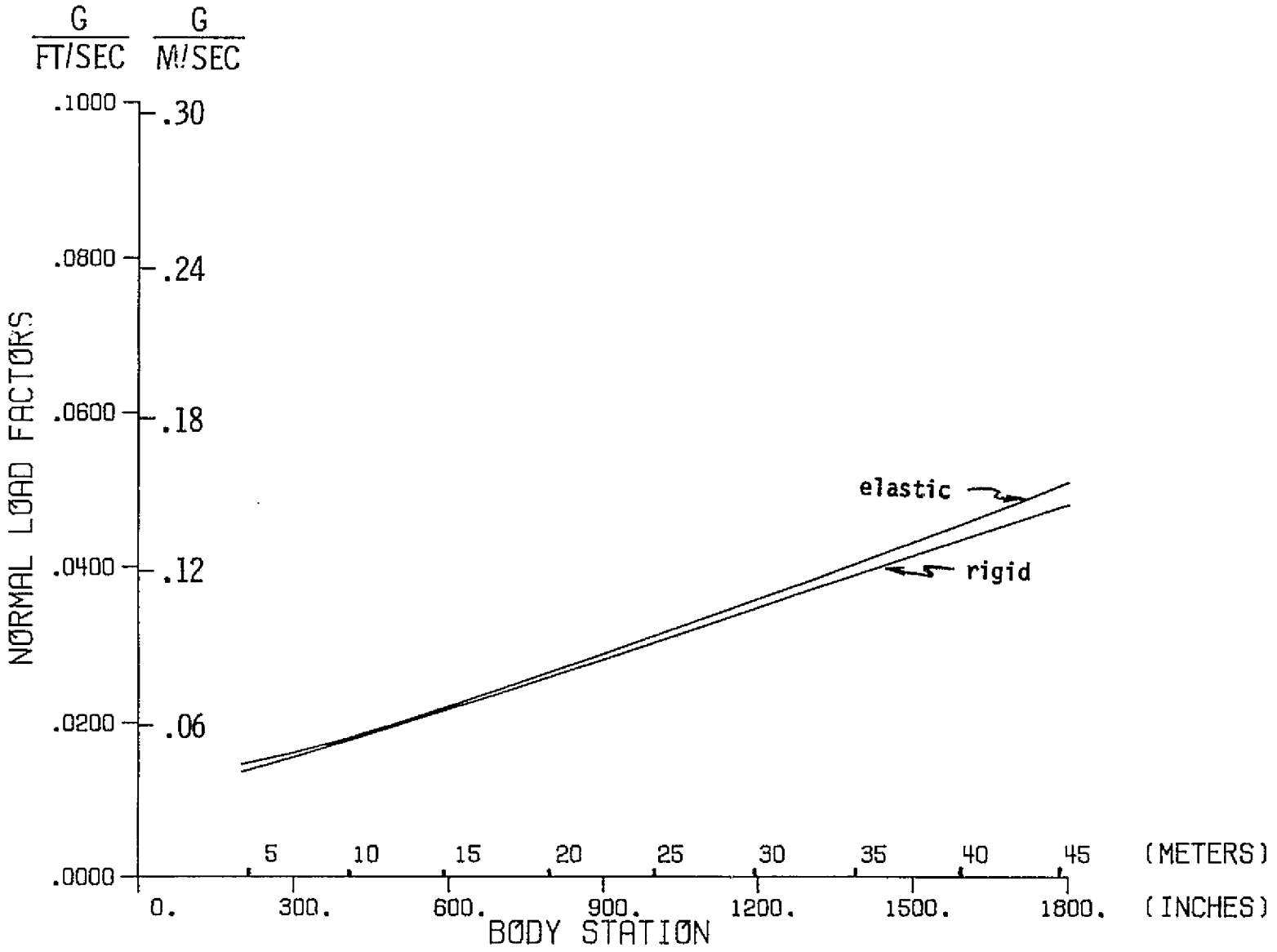

Figure C.2 B-52H Load Factors, Case #5. Mach .55, Altitude 610 m (2000 ft).

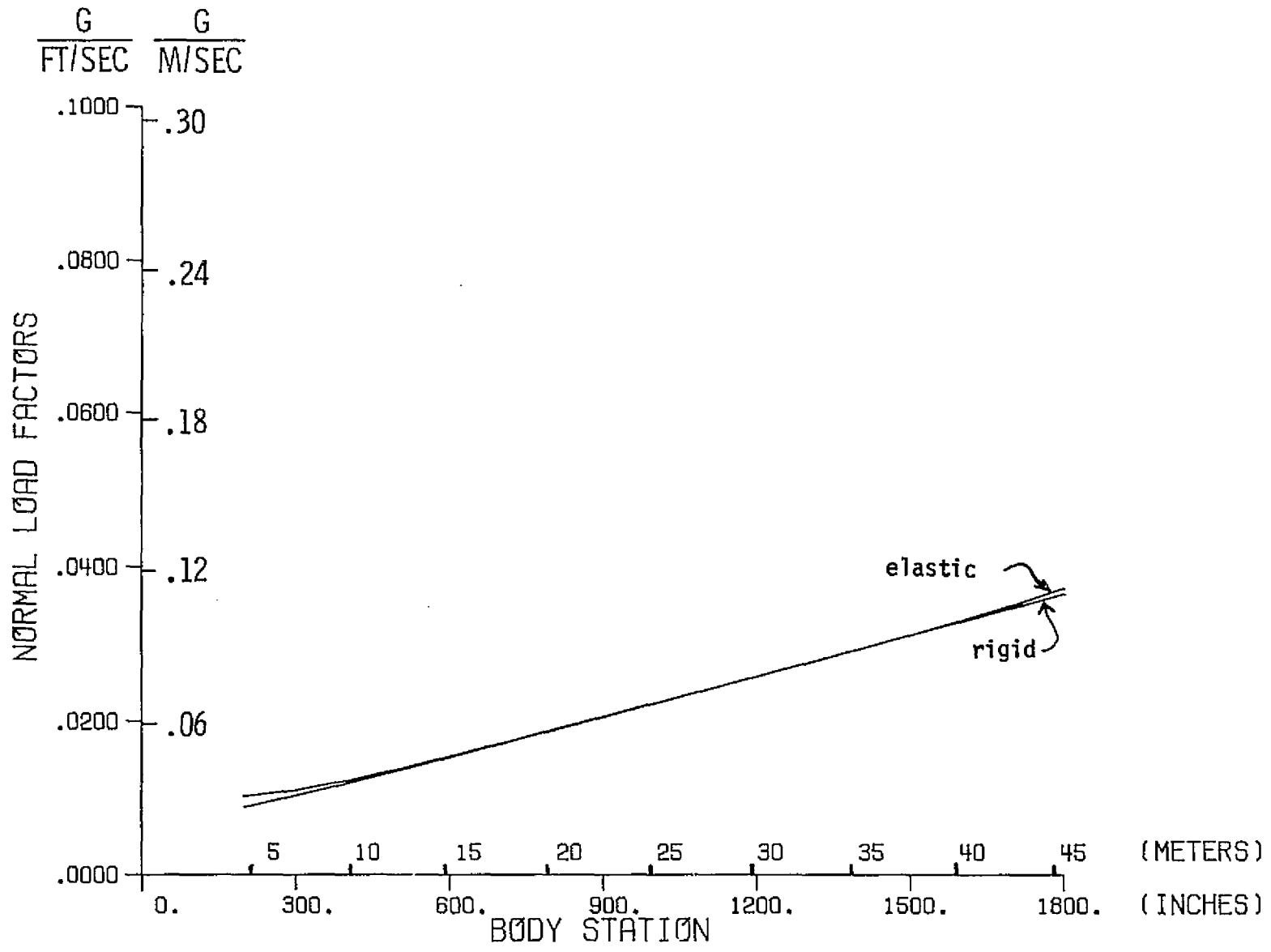

Figure C.3 B-52H Load Factors, Case #6. Mach .55, Altitude 610 m (2000 ft).

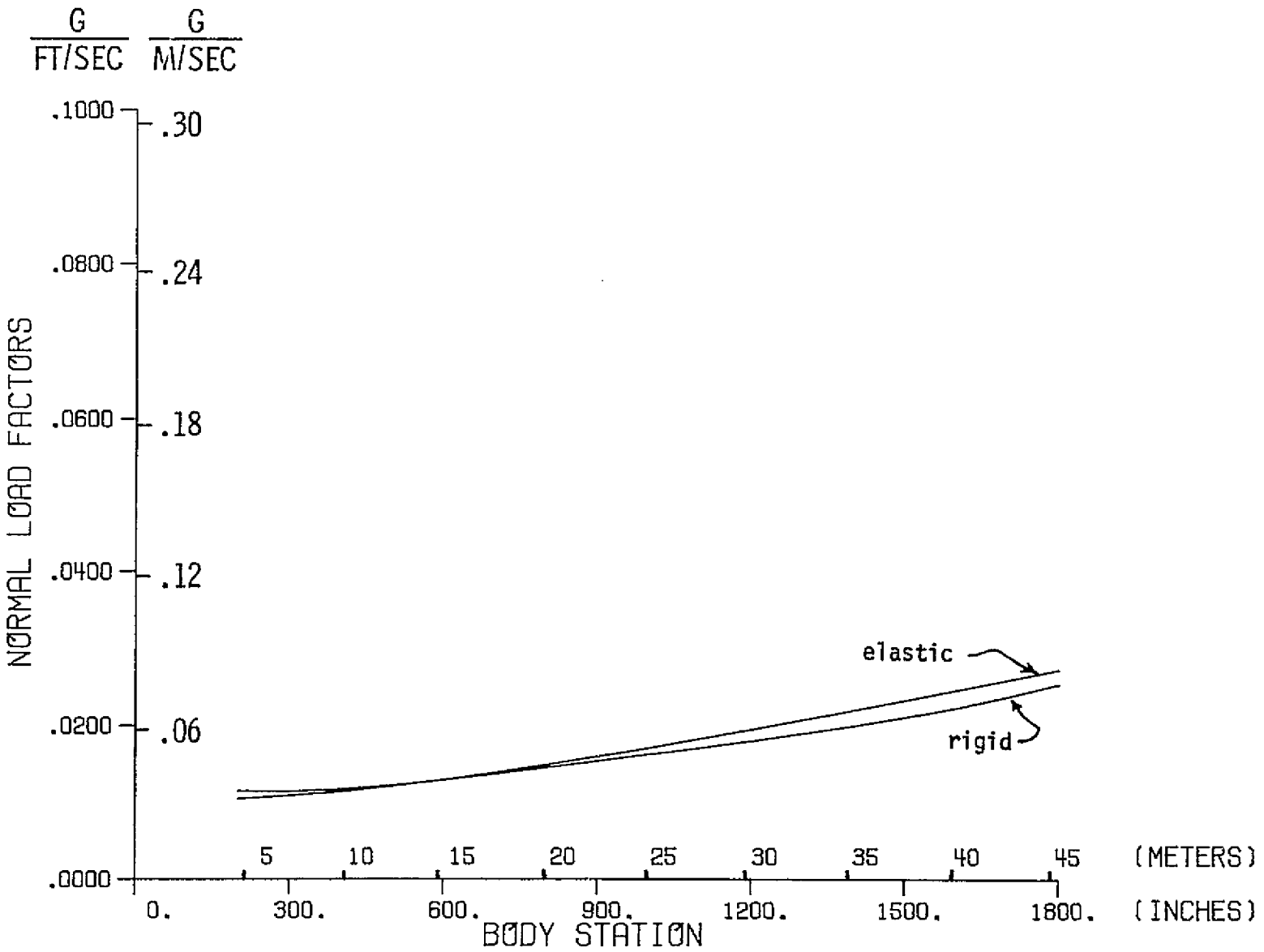

Figure C.4 B-52H Load Factors, Case #12. Mach .55, Altitude 610 m (2000 ft).

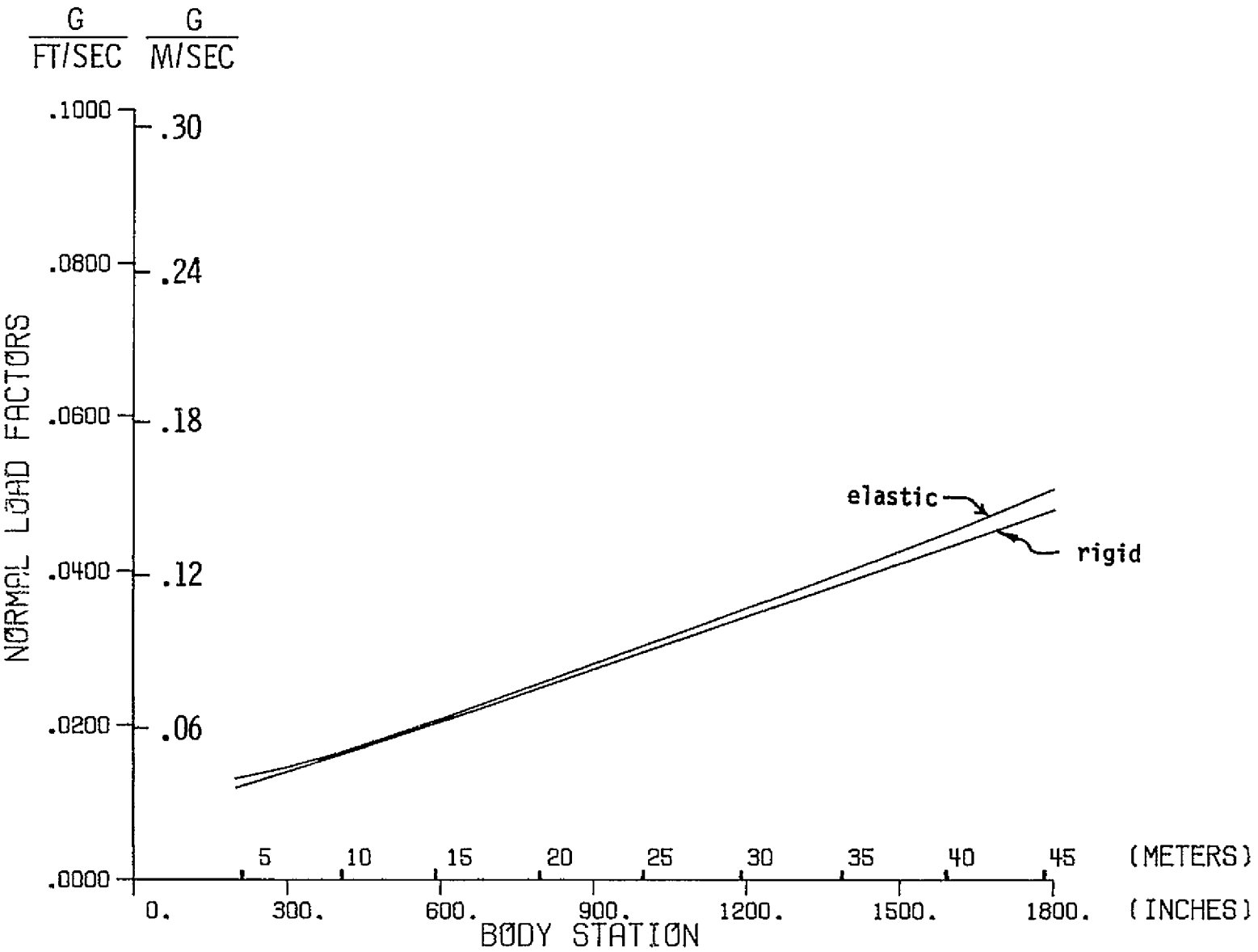

Figure C.5 B-52H Load Factors, Case #14. Mach .55, Altitude 610 m (2000 ft).

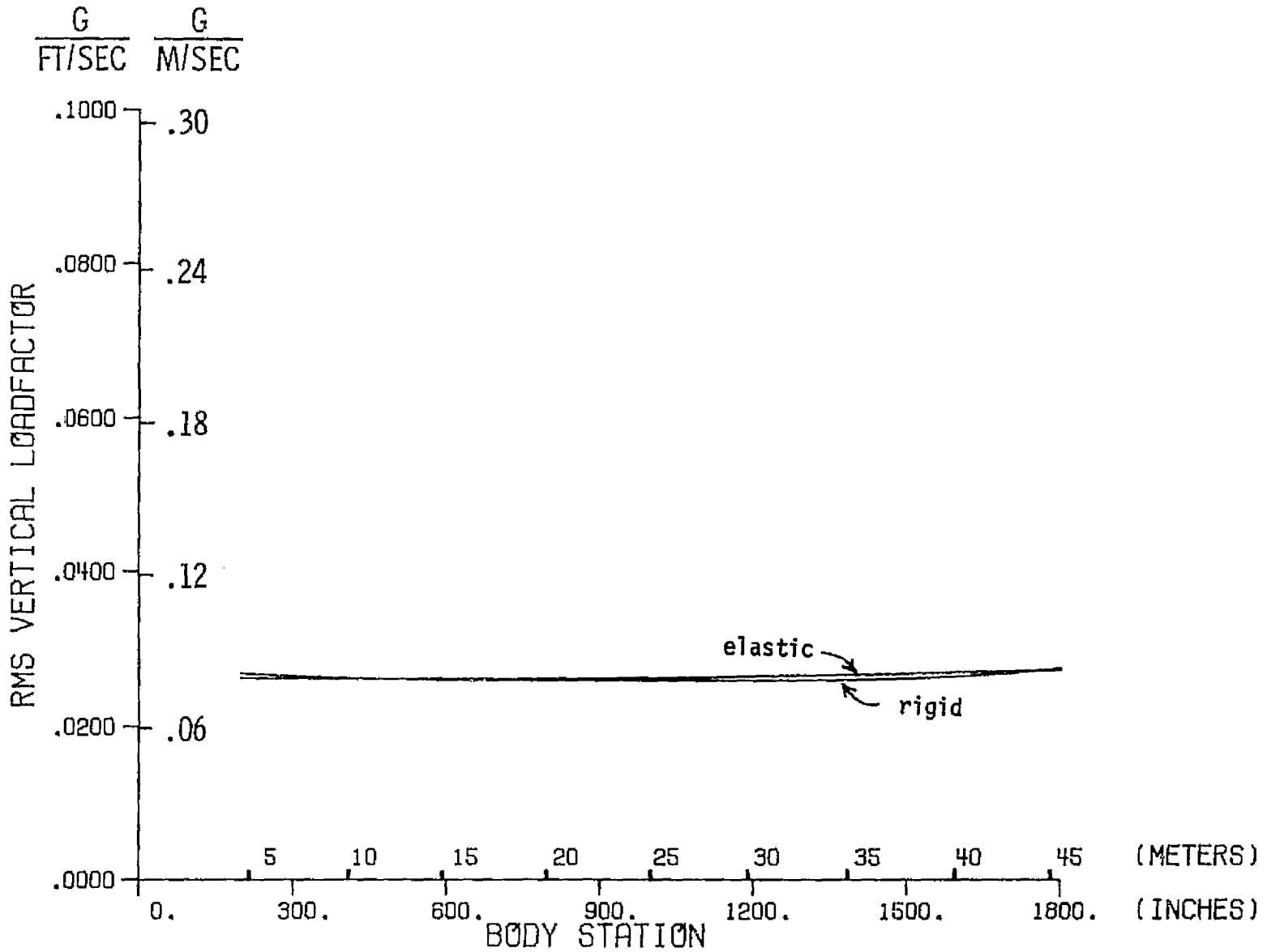

Figure C.6 B-52H Load Factors, Case #37. Mach .55, Altitude 610 m (2000 ft).

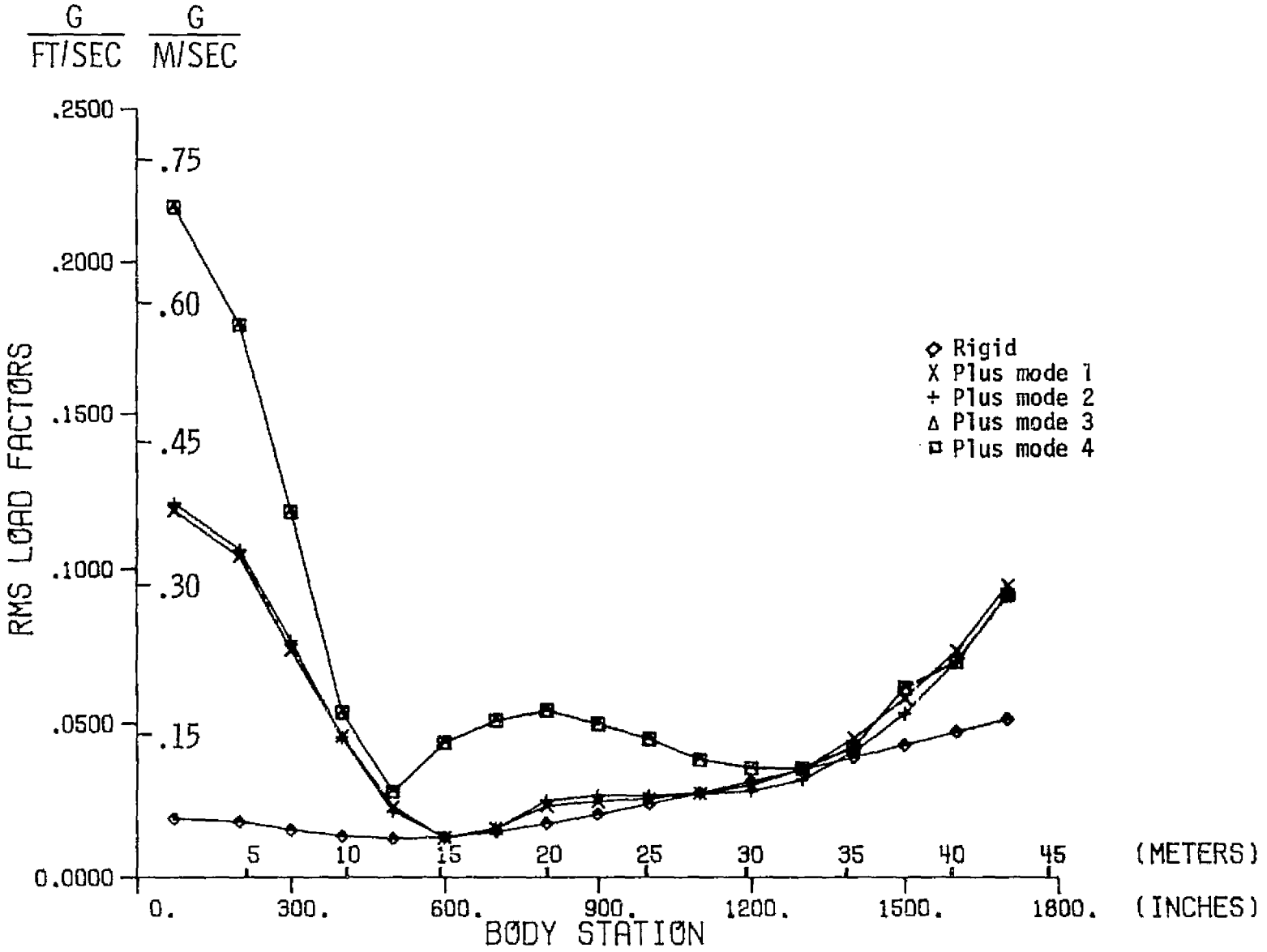

Figure C.7 B-1 Load Factors, Case #4. Mach .85, Altitude 30 m (100 ft).

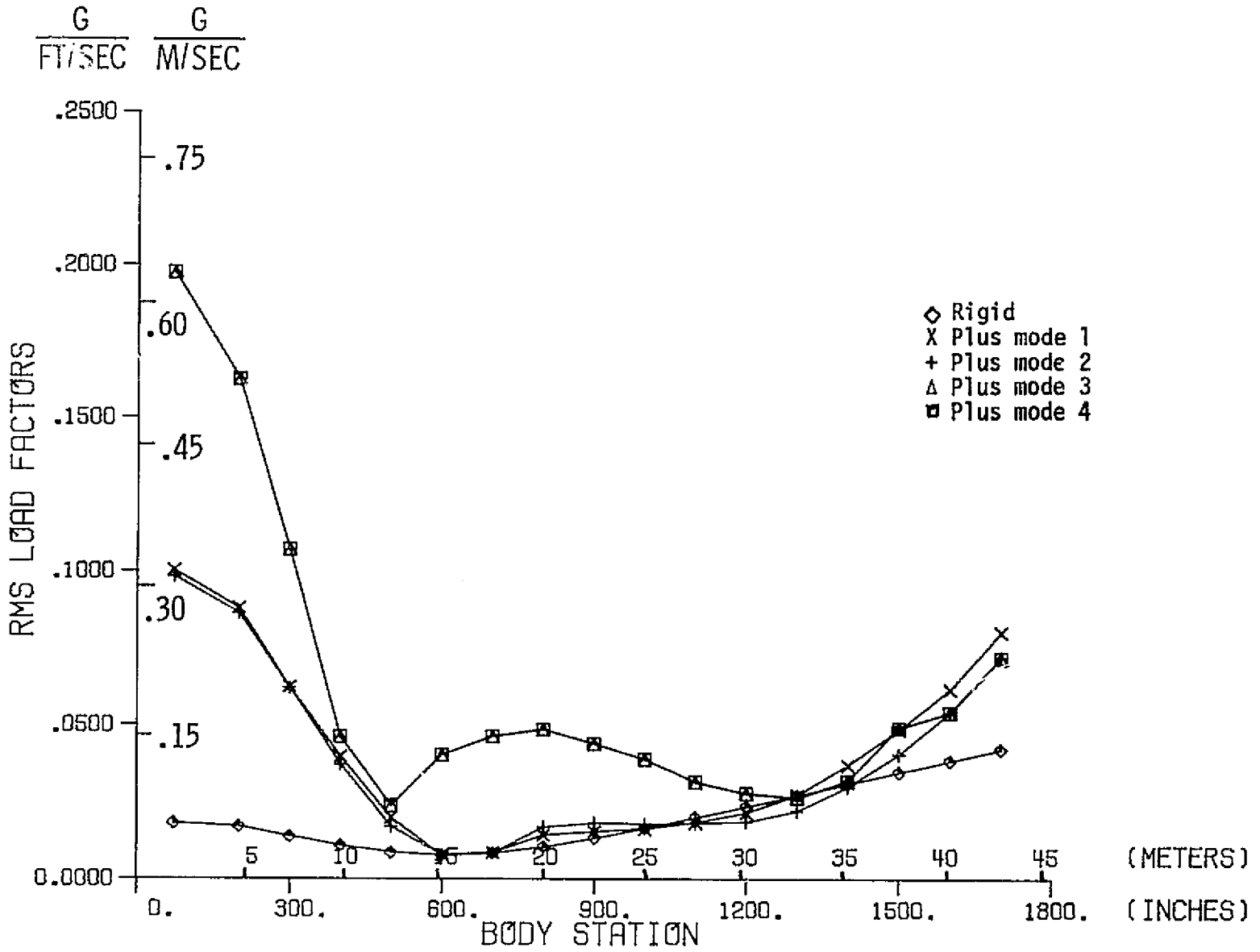

Figure C.8 B-1 Load Factors, Case #18. Mach .85, Altitude 30 m (100 ft).

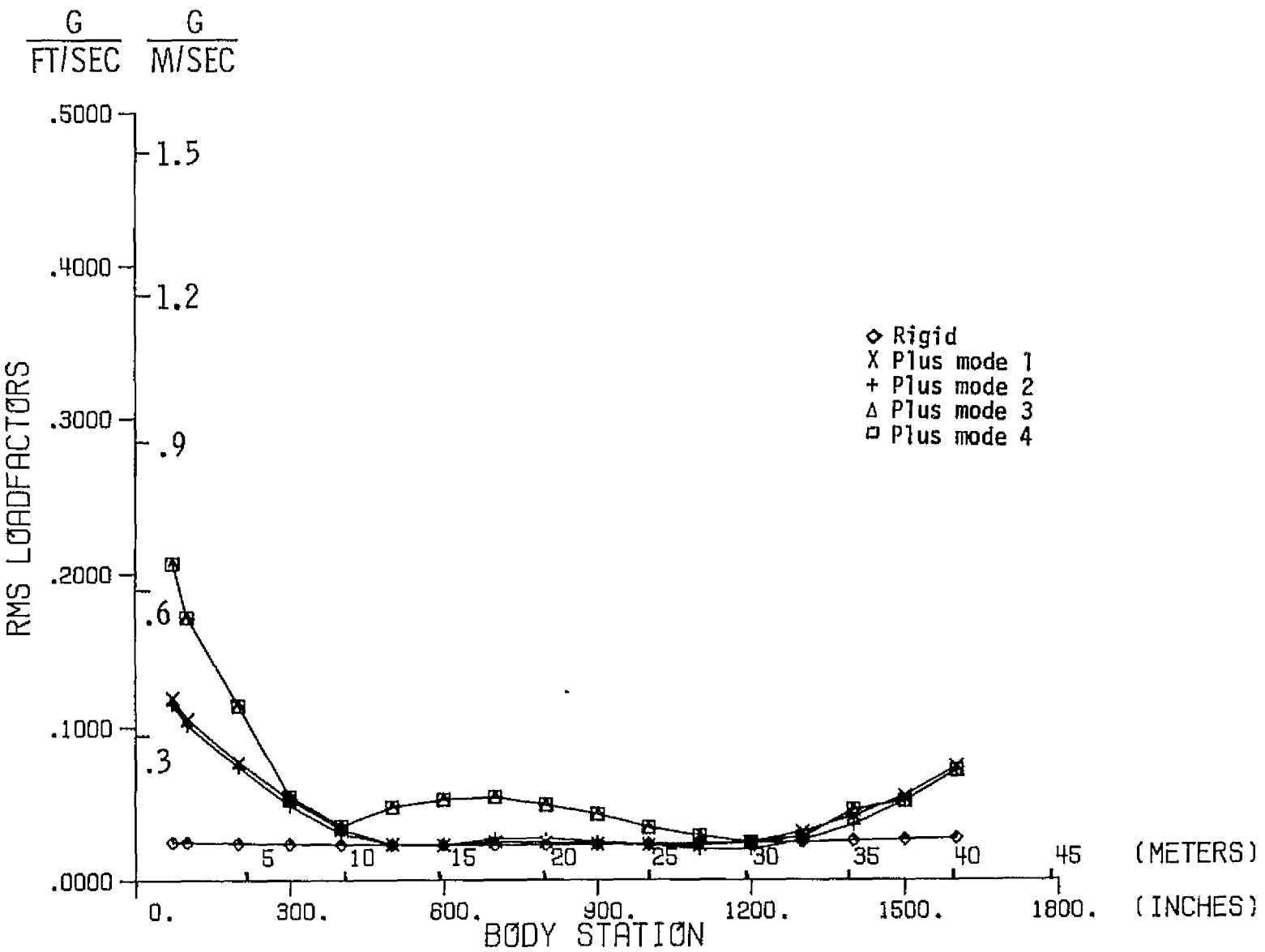

Figure C.9 B-1 Load Factors, Case #32. Mach .85, Altitude 30 m (100 ft).